Applications of Responsive Assembly and Disassembly of Colloids

by

Yuning Liu

A thesis submitted in partial fulfillment of the requirements for the degree of

Master of Science

Department of Chemistry
University of Alberta

Abstract

The processes of assembly and disassembly of colloids has rapidly grown in interest over the decades. Assembly and disassembly are able to respond to the changes in conditions, which makes them important in sensing and stimuli-reponsive processes. There are two applications based on assembly and disassembly processes respectively in this thesis. In one example, fuel is used to drive the dissipative assembly process of forming spherical micelles by molecules that are temporarily mode amphipathic by the addition of fuel. In the other, oligouncleotidess triggered the disassembly of DNA modified gold nanoparticles , which leads to a colour change allowing the method to be able to detect biomarkers.

In Chapter 2, the dissipative amphipathic molecules are synthesized by copper (I)-catalysed azide–alkyne cycloaddition (CuAAC). These amphipathic molecules are able to self-assembly to spherical micelles by consuming a chemical fuel such as 1-ethyl-3-(3-dimethylaminopropyl)carbodiimide (EDC). The process of self-assembly and dissipation of micelles is determined by analytical methods, such as fluorescence, dynamic light scattering, and transmission electron microscopy.

In this study of disassembly in Chapter 3, we combine DNA-gold nanoparticle aggregates with an amplification method to detect RNA biomarkers. The DNA amplicons are able to trigger the disassembly of DNA-gold nanoparticles to achieve a colorimetric detection. In addition, selectivity experiments show that colorimetric detection can distinguish the target RNA with single-base mismatch RNA and non-match RNA. Also, target RNA spiked in human lungs total RNA can also be detected by this method. Afterwards, we reduced aggregates to improve the sensitivity of our method.

In chapter 4, we provide some ideas to further explore the research described in this thesis. These future works focus on the optimization of the applications in assembly and disassembly processes.

Preface

This thesis is the original work by Yuning Liu and the research was highly collaborative. Chapter 2 was an international collaboration project, and the idea was conceived by Dr. Job Boekhoven (Technical University of Munich) and Dr. Julianne Gibbs (University of Alberta). This project was mainly performed in the Boekhoven lab in Munich, Germany. Dr. Marta Tena-Solsona provided some guidance of HPLC gradient and fluorometer conditions. Raphael Grötsch helped me to set up the measuring condition of dynamic light scattering. I was responsible for the synthesis of the molecules. Also, I collected data and analyzed the results included in this chapter. The TEM images were taken by Caren Wanzke. Raphael Grötsch took over this project to optimize this work after I left Germany. This project is being written into a manuscript by Dr. Job Boekhoven, Dr. Julianne Gibbs, and Raphael Grötsch. Portions of Chapter 2 were taken from this manuscript.

RNA triggered lesion-induced DNA amplification described in Chapter 3 was developed and mostly operated by B. Safeenaz Alladin-Mustan. DNA-gold nanoparticle aggregate preparation and colorimetric detection related to this chapter were performed by me. Additionally, B. Safeenaz Alladin-Mustan performed and analyzed PAGE gels. In this thesis, only the kinetic traces were shown while the original gel figures were not included. The colorimetric figures were shot by an iPhone 7 and organized by me. Parts of this chapter appear in a manuscript in preparation by B. Safeenaz Alladin-Mustan and Dr. Julianne Gibbs. This manuscript is currently being modified following reviewers' suggestion.

Acknowledgements

I would like to express my gratitude take this chance to express my gratitude to all those helped me during my graduate study.

My deepest gratitude goes to my supervisor Professor Julianne Gibbs for her constant patience, encouragement, and guidance throughout my journey of Master study. This multidisciplinary group expanded my knowledge in chemistry. Her training improved my skills in article summary, presentation, and academic writing. I am very thankful to her for giving me the opportunity to work in projects related to different divisions in chemistry. Also, I appreciate that her help in the editing on my thesis.

I would also like to thank Prof. Mark McDermott and Prof. Robert Campbell for being in the supervisory committee and for providing valuable suggestions during my graduate studies. I wish to thank Dr. Christopher Cairo for serving as my defense examination member.

Furthermore, thanks for Alberta / Technical University of Munich International Graduate School for Hybrid Functional Materials (ATUMS) program, operated by Prof. Jonathan Veinot and Leah Veinot for providing me funding and the opportunity to join this amazing program which helped me improve my soft skills and complete my exchange research at the Technical University of Munich (TUM), Germany. Also, I am grateful that Mitacs that offered mefunding to support my three-month exchange in Munich. With gratitude, I like to express my warm thanks to Prof. Job Boekhoven for hosting me in laboratory at TUM and giving me a chance to learn more about knowledges in supramolecular. Also, the valuable suggestions provided by him helped me to finish an international project.

I am also deeply indebted to everyone that I am lucky enough to work with during my Master study. In the Gibbs group, I would like to specially thank B. Safeenaz Alladin-Mustan for her

guidance and collaboration of performing DNA/RNA amplification experiments. I would also like to thank Dr. Eiman Osman for her initial training of DNA operation as well as her suggestions of writing thesis. I should mention Hansol Park for helping me to complete the NMR measurements. Also, thank her for taking over all of my group jobs when I exchanged in Munich. I would like to thank to Jisu An for the help with the DNA structure project. I would also like to give my appreciation for the other past and present group members of Gibbs group, namely, Dr. Emma Kerian, Dr. Zhiguo Li, Dr. Akemi Darlington, Benjamin Rehl, Mokhtar Rashwan, Shyam Parshotam, Luca Maiorana, Sun Kim, Anyeld Ubeda, Sarah Hales, Hoi Pui (Emily) Chao, Gunwant Matharu, and Tianli Liu. Thank everyone for all help and advice of academic and non-academic issues. I also thank Mario Schmidt from Dr. Sarah Styler group for the help for the training and advice with HPLC.

Besides, I also thank Scientific Services at the Department of Chemistry. I would like to specially express my deep thanks to Gareth Lambkin in Biological Services for his suggestion in biological techniques and training me with different instruments. I would also like to thank Dr. Randy Whittal and Jing Zhang for their help for mass spectrometry. Also, I thank Wayne Moffa for helping me with the elements analysis.

Also, I would like to thank the Boekhoven's group for their help. Specially, I would like to thank Dr. Marta Tena-Solsona for the guidance of advanced materials and training of instruments. I would mention Raphael Grötsch for giving the instruction of dynamic light scattering and taking over the micelle project after I left Germay. I would also like to thank Caren Wanzke for helping to image by cyto-EM. I also like to express my thanks to rest of Boekhoven's group: Benedikt Rieß, Fabian Schnitter, Patrick Schwarz, Carsten Donau, Kun Dai, Alexander Bergmann, Laura Tebcharani, Sebastian Auffarth, Christine Kriebisch, Brigitte Kriebisch, and Tabea Huss.

I would like to specially thank my roommate Sarpkan Demirer and his parents, Ozlem Demirer and Suat Demirer, for letting me feel at home in Edmonton. Also, thank the small family member Cookie the cat for helping me to reduce pressures.

Finally, I would like to express warmest thanks to my mother (Ningzhi Luo) and father (Zunde Liu) for their constant support and inspiration to motivate me during the period of Master program.

Table of Contents

List of Tables

List of Figures

List of Abbreviation/symbols

Ab	**Abasic**
AuNP	Gold nanoparticle
C8E4	Tetraethylene glycol monooctyl ether
cDNA	Complementary deoxyribonucleic acid
Chi	Chitosan
CMC	Critical micelle concentration
Cryo-EM	Cryogenic- transmission electron microscopy
CTAB	Cetyl trimethylammonium bromide
CuAAC	Cu(I)-catalyzed azide/alkyne cycloaddition
dDNA	Displacement deoxyribonucleic acid
DLS	Dynamic Light Scattering
DMT	Dimethoxytrityl
DNA	Deoxyribonucleic acid
DOPA	1,2-dioleoyl-sn-glycero-3-phosphate
dsDNA	Double stranded deoxyribonucleic acid
DTT	Dithiothreitol
EDC	1-ethyl-3-(3-dimethylaminopropyl)carbodiimide
Egg PC	l-α-phosphatidylcholine
EPA	4-ethynylphthalic acid
EPAn	4-ethynylphthalic anhydride

ESI-MS	Electrospray ionization mass spectrometry
FAM	Fluorescein
H. pylori	*Helicobacter pylori*
HCR	Hybridization chain reaction
HLTR	human lungs total ribonucleic acid
HPLC	High-performance liquid chromatography
LAMP	Loop mediated DNA amplification
LIDA	Lesion induced DNA amplification
LOD	Limit of detection
MALDI-TOF	Matrix-assisted laser desorption/ionization -time-of-flight
MES	2-(N-Morpholino)ethanesulfonic acid
miRNA	Micro-ribonucleic acid
mmRNA	mismatched ribonucleic acid
NEANA	Nicking endonuclease assisted nanoparticle amplification
Nease	Nicking endonuclease
NHS	N-hydroxysuccinimide
NIR	Near-infrared
NMR	Nuclear magnetic resonance
nmRNA	non-matched ribonucleic acid
NP	Nanoparticle
NPCs	Nanoparticle clusters
NR	Nile red
OTA	Ochratoxin A

PAA	Poly(acrylic acid)
PBS	Phosphate buffered saline
PCR	Polymerase chain reaction
TEG-Azide	1-azido-2-(2-(2-methoxyethoxy)ethoxy)ethane
PES	Polyethersulfone
PS	Polystyrene
RCA	Rolling circle amplification
RNA	Ribonucleic acid
SiCN	Silicon nanocrystal
SPA	Spherical nucleic acids
SPR	Surface plasmon resonance
ssDNA	Single stranded deoxyribonucleic acid
TEM	Transmission electron microscopy
TFA	Trifluoroacetic acid
THF	Tetrahydrofuran
λ	Wavelength

Chapter 1

General Introduction

1.1 Introduction to self-assembly of colloids

Self-assembly is a spontaneous process from simplicity and disorder to complexity and order. This process can take place at both small and large scales, from crystallization of molecules to weather systems.[1] Research related to self-assembly has rapidly increased over three decades. For example, researchers have studied the self-assembly relevant to biology, such as the formation of the phospholipid bilayer of membranes.[2] Therefore, it is an important step for understanding life. Whitesides and coworkers classified self-assembly into two main groups: static self-assembly and dynamic self-assembly.[3] The formation of static self-assembly reaches equilibrium when the ordered structure appears, such as protein folding. But in dynamic self-assembly, the structure forms when the system is forced out of equilibrium by continuous energy dissipation, which is often found in biological systems.[3] Scientists have focused mainly on static self-assembly although dynamic assemblies are gaining wider attention.[4-7]

Colloids are particles with diameters between 1 nm and 1000 nm dispersed in a medium, and they can result from static self-assembly of molecules into different shapes and structures. Molecular scale assembly involves non-covalent or weak covalent interactions, including Van der Waals,[4] hydrogen bonds,[5] coordination bonds,[6] and π-π stacking.[7] Altering one or more of those forces may break the balance of assembly, leading to the transformation of structures. Colloids can be classified into hydrophilic colloids and hydrophobic colloids. A hydrophilic colloid is attracted by water while a hydrophobic colloid is repelled by water. Therefore, colloidal particles may have a different assembled structure in different solvents.[8] Researchers have reported assembly systems based on hydrophilic/hydrophobic property.[9-10]

1.2 Responsive assembly based on hydrophobic interactions

1.2.1 Self-assembly of amphipathic molecules

One main group of responsive self-assembly molecules is amphipathic molecules, such as surfactants. Amphipathic molecules are composed of a hydrophilic fragment and a hydrophobic chain and their self-assembly in water through hydrophobic interactions plays a significant role in biological systems such as lipid bilayers.[2, 11] When the concentration is higher than the critical micelle concentration (CMC), hydrophobic chains avoid contact with water molecules by coming together to form a core surrounded by a hydrophilic shell.[12] A typical structural example is a micelle, and amphipathic molecules are able to form different shapes depending on their structures of micelles, such as spherical micelles,[13] wormlike micelles,[14] hexagonal liquid crystals,[15] etc.

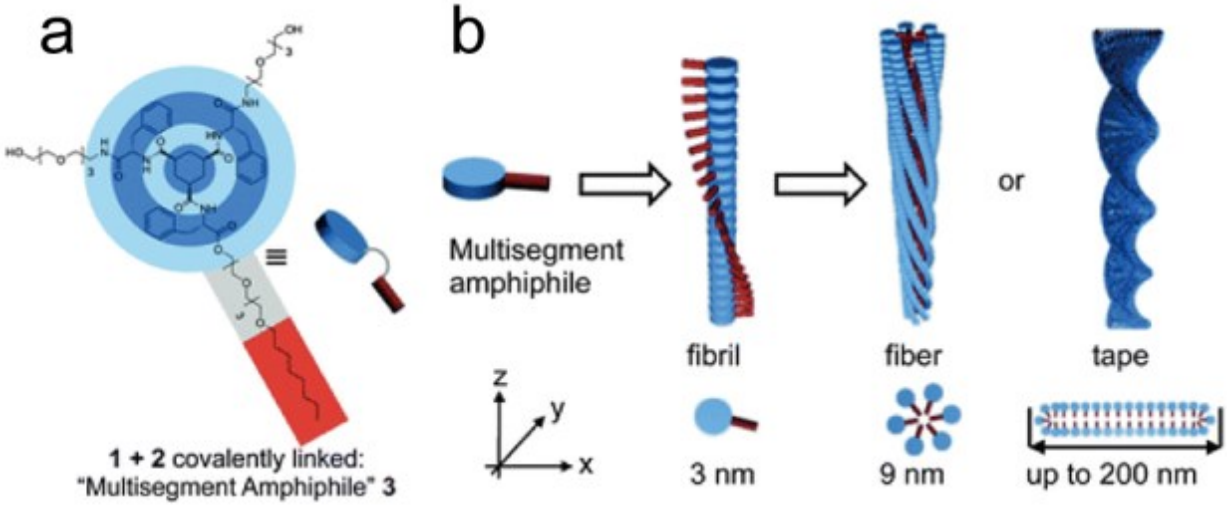

Figure 1. 1 (a) The structure of multisegment amphiphile. (b) The illustration of formation of hierarchical structures by different concentrations of the multisegement amphiphile. Image reproduced with permission from ref. 16. Copyright © 2010 The Royal Society of Chemistry.

Amphipathic molecules not only participate in micelle formation but also other complicated nanostructures by modifying or adding functional groups to change the hydrophilicity. For

example, Boekhoven et al. developed a multisegment amphiphile based on the covalent connection between a micelle forming surfactant tetra-ethylene glycol mono-octyl ether (C4E8) and a gelator 1,3,5-cyclohexyltrisamide group.[16] C4E8 is an amphipathic molecule that is able to form a spherical micelle while 1,3,5-cyclohexyltrisamide can form worm-like micelles. They observed different helical nanostructures forming by controlling concentration of the new multisegment amphiphile. The smallest assembly structure was a 3 nm fibril that was able to aggregate into 9 nm fibers and 50-200 nm tapes (Figure 1.1).[16]

1.2.2 Self assembly of hydrophobic metal nanoparticles

Hydrophobic interactions have also been used to assemble hydrophobic metal nanoparticles into colloidal aggregates. For example, a method for assembling nanoparticle clusters (NPCs), a type of aggregate, was designed by Qiu et al.[9] They used cetyl trimethylammonium bromide (CTAB) as surfactant to create an oil-in-water emulsion system. Hydrophobic nanoparticles made of Fe_3O_4 were synthesized in the oil phase and CTAB was in the aqueous phase. The idea is that oil would be suspended in water as tiny droplets. Moreover, the hydrophobic nanoparticles could be included in these oil-in-water droplets as they were covered by CTAB due to hydrophobic interactions.[17] The oil phase removal by evaporation led these nanoparticles to form larger spherical clusters. Based on this strategy, they achieved almost 100% yield of assembly (Figure 1.2).[9]

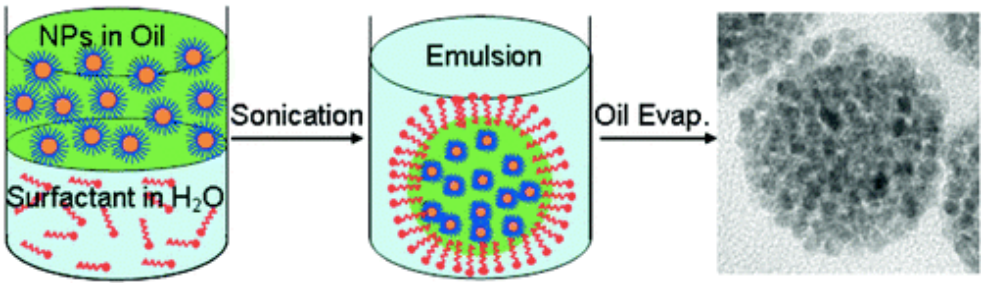

Figure 1. 2 A schematic illustrating the assembly process of hydrophobic nanoparticles. Nanoparticles were dispersed in oil and the surfactant CTAB was in water layer. After emulsion, the surfactant covered nanoparticles formed aggregates. The TEM image showed the aggregates after evaporating. Image reproduced with permission from ref. 9. Copyright © 2010 American Chemical Society

Gold nanoparticles (AuNP), also called colloidal gold, are one of most popular nanomaterials over 25 years. Generally, the diameter of a AuNP is 1 - 100 nm when synthesized by the common Turkevich method,[18] where the size is controlled by adjusting the ratio of the sodium citrate reducing agent and chloroauric acid ($HAuCl_4$). Researchers have synthesized gold nano-stars,[19] nano-cages,[20] and nano-rods[21] by modern methods, which has led to materials with different properties owing to dependence of many properties of nanostructures on their size and shape. For example, a special property of AuNPs is their surface plasmon resonance (SPR), which is the oscillation of electrons at the interface stimulated by the absorbance of specific wavelengths of visible light over a narrow range. The range of absorption peaks of spherical gold nanoparticles are between wavelengths of 500 nm to 550 nm, this absorbance maximum undergoes a redshift with colour change from red to purple upon an increase in the nanoparticle diameter[22] or upon nanoparticle aggregation.[23]

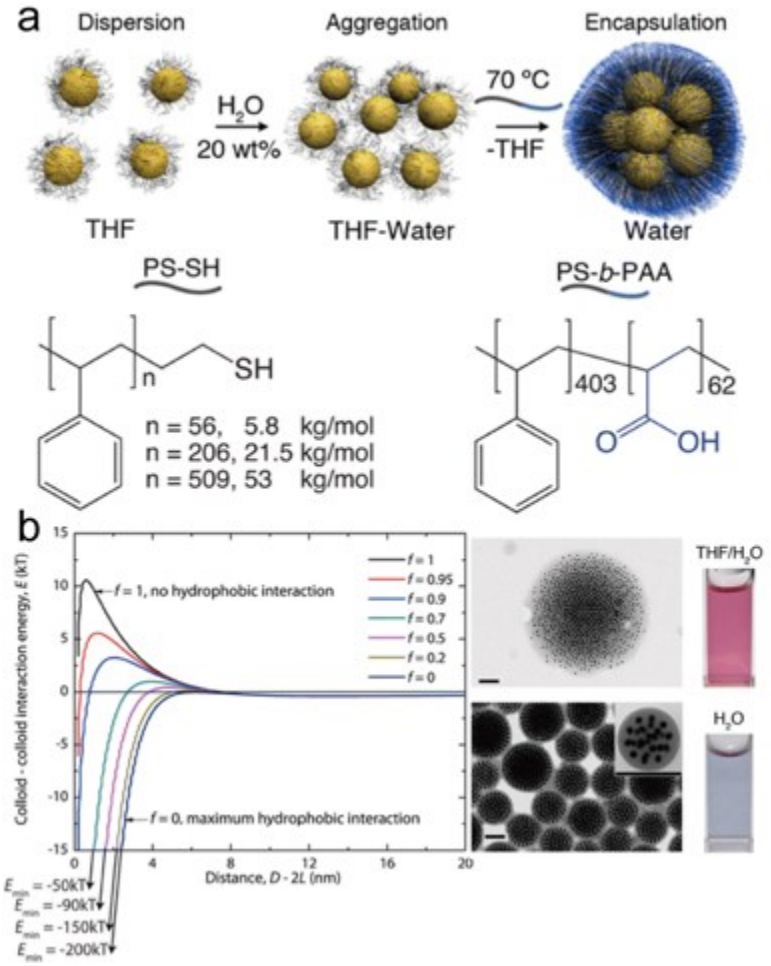

Figure 1. 3 (a) Scheme illustrating the assembly of PS modified gold nanoparticles after addition of 20 wt% of water and encapsulating by adding surfactant and evaporating off the THF. (b) Colloid-colloid interaction energy E as a function of interparticle distance D. When the THF solvent fraction f=1, there is no hydrophobic interactions leading to no aggregation. The hydrophobic interaction increases as f decreases from 1 to 0. Polymer encapsulation keeps the nanoparticles stable in THF/water mixtures but the colour in purple shows visible aggregates in 100% water (f=0). Scale bars: 200 nm. Images adapted and modified with permission from ref. 24. Copyright © 2012 American Chemical Society

Another advantage of gold nanoparticles is they can be functionalized by different molecules containing a thiol functional group. By modifying the gold nanoparticle with polystyrene (PS) that contained a thiol modification, Sanchez-Iglesias and coworkers established

a methodology for nanoparticle aggregation in water.[24] Specifically, PS-coated gold nanoparticles were dispersed in a tetrahydrofuran (THF) solution and aggregated by addition of water into THF. In addition, a amphiphilic surfactant, comprising hydrophobic (PS) and hydrophilic poly(acrylic acid) (PAA) blocks, was added to stop the growth of clusters. Just like in the previous example with CTAB,[9] hydrophilic PAA at the surface was able to stabilize the micelle structure and sequester the particles into water (Figure 1.3a). As shown in Figure 1.3b, in the absence of water when the solvent ratio f equaled 1 (pure THF) the largest positive colloid-colloid interaction energy showed the best tendency of colloid separation as there was no hydrophobic interaction. The reason is that colloids with a high interaction energy tend to repulse until the energy reduces to zero.[25-26] However, when the percentage of water increased (f<1), the nanoparticles tended to aggregate owing to the increase in hydrophobic interactions leading to a decrease in interaction energy.[24]

1.3 Introduction to DNA nanostructures

1.3.1 DNA origami nanostructures from programmed assembly of DNA

Deoxyribonucleic acid (DNA) is often selected as a component in assemblies and nanoswitch devices due to the DNA secondary structure, also called a double helix or duplex. Two complementary strands of DNA assemble to form a spiral structure based on the unique combinations of the four nucleobases of DNA, namely adenine (A), thymine (T), cytosine (C), and guanine (G). The highly selective Watson-Crick complementarity can be applied to build new nanostructures.[27] Accordingly, researchers have built 2D and 3D nanostructures with a variety of sizes and shapes.[28] For instance, Rothemund and co-workers used a long single DNA strand which is able to fold into a desired pattern.[29] Using this strategy, the authors were able to build rectangles, faces, stars and other patterns (Figure 1.4a).[29] A publication by Anderson and coworkers reported

the self-assembly of a three-dimensional $42 \times 36 \times 36\ nm^3$ DNA box where they used a single strand DNA of M13 bacteriophage to fold six into interconnected sheets. DNA duplexes built the six sheets and each edge was formed by a stable hairpin between two adjacent faces (Figure 1.4b).[30]

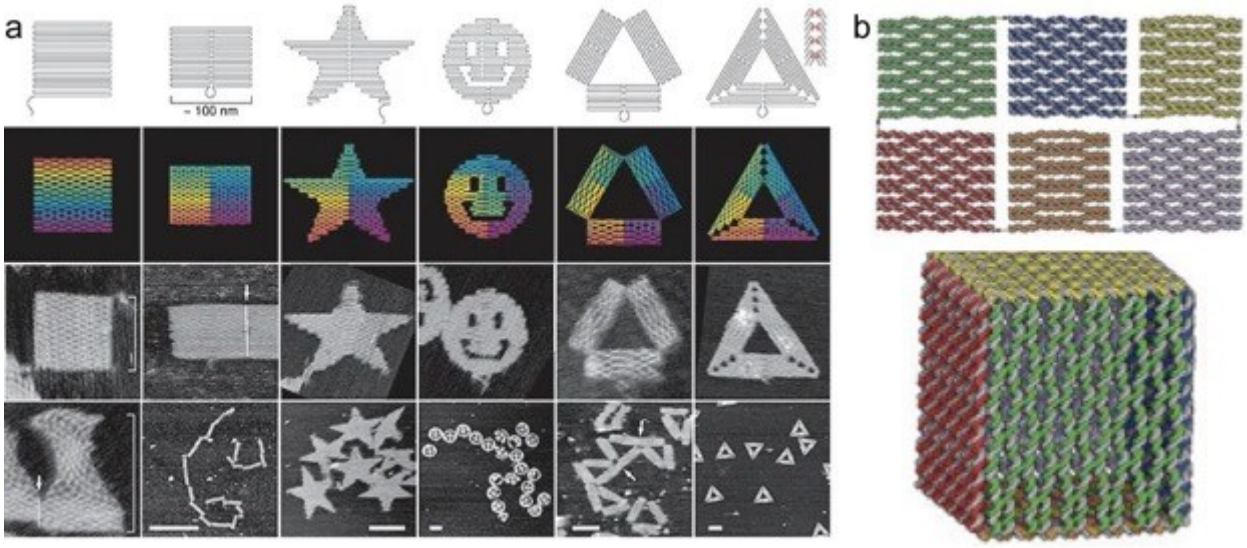

Figure 1. 4 (a) Atomic force microscopy (AFM) images of different DNA origami structures. Scale bars: 100 nm. (b) Six DNA sheets in a flat and cubic structure, respectively. Image in (a) reproduced with permission from ref. 29. Copyright © 2006, Springer Nature. Image in (b) adapted and modified with permission from ref. 30. Copyright © 2009, Springer Nature.

1.3.2 DNA templated assembly with DNA-conjugated nanomaterials

DNA has also been used as a template for the construction of self-assemblies of nanostructures, which play a significant role in biosensors and gene delivery[27, 31-32] In the 1990s, scientists developed DNA-modified gold nanoparticles (DNA-AuNPs) that they synthesized from 13 nm gold nanoparticles functionalized with terminal modified thiol DNA to form DNA-gold nanoparticles complexes, which they subsequently referred to as spherical nucleic acids (Figure 1.5a).[33] The DNA could be a template to aggregate nanoparticles due to its ability to form a double helix even when attached to the surface of a AuNP.[34-35] Jin et al. used a DNA strand as a linker to

hybridize with two complementary DNA coated on gold nanoparticle surfaces (Figure 1.5b).[34] Different structures were achieved based on thermal conditions. Generally, aggregates formed below the dissociation temperature of the DNA duplex linking the DNA-AuNP, while dispersed colloids were present above. As shown in Figure 1.5c, Nykypanchuk et al. directly used two partly complementary DNA strands to modify gold nanoparticles, respectively. By adjusting the DNA length, they also developed a method to control the amorphous and crystalline aggregation.[35]

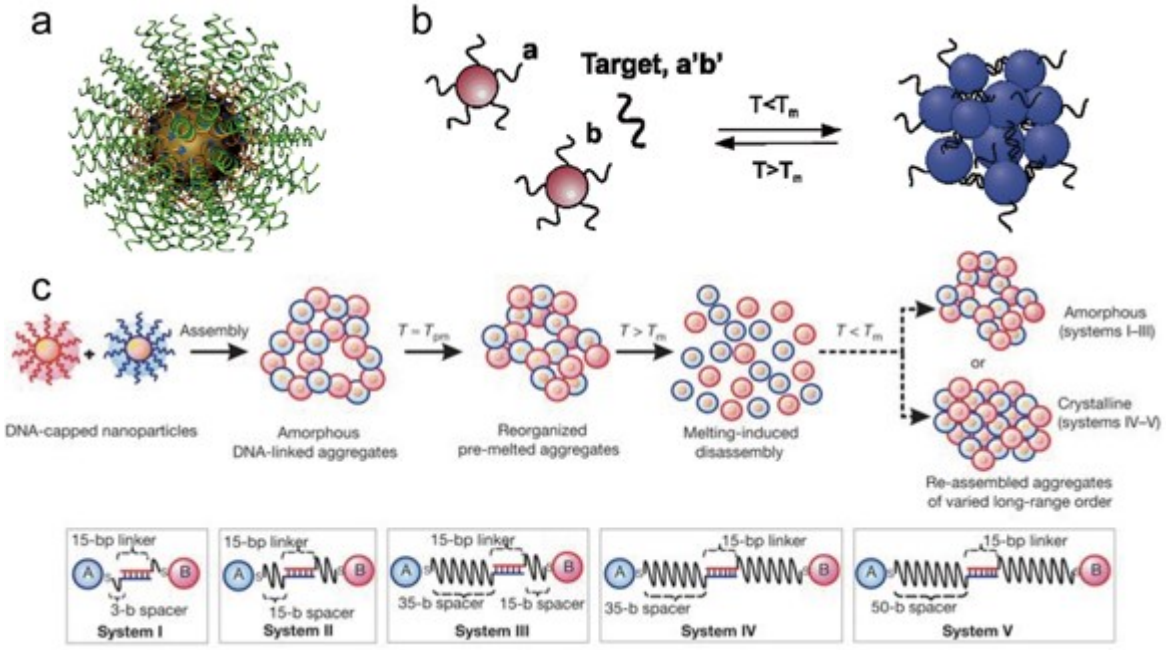

Figure 1. 5 (a) The structure of spherical nucleic acids (SPA). (b) Scheme illustrating the assembly system of DNA-AuNPs, which leads to a change in colour of the gold nanoparticle colloids from pink to blue/purple. (c) DNA hybridization of two complemenatry DNA-AuNP. Controlling the length of DNA including the spacer sequence allows one to build amorphous or crystalline aggregates of AuNP. Image (a) reproduced with permission from ref. 33. © 2012, American Chemical Society. Image (b) reused with permission from ref. 34. Copyright © 2003, American Chemical Society. Image (c) adapted with permission from ref. 35. Copyright © 2008, Springer Nature.

This strategy has been applied in mRNA, small molecule, ion, and protein detection.[36] For example, gold nanoparticles were used in detection of Hg^{2+} by a mercury induced hybridization (Figure 1.6).[37] This assemby system took advantage of the ability of T:T mismatches within a duplex to react with Hg^{2+} to form a thymine-Hg^{2+}-thymine complex (T-Hg^{2+}-T). They designed a thymine rich linker and two complementary DNA probe strands attached to gold nanoparticles; where the template and probes could hybridize to form duplex with T:T mismatches. When the mercury ions were present, Hg^{2+} selectively bound with T-T mismatches, resulting in the formation of stable T-Hg^{2+}-T complexes. It led to nanoparticle aggregation and colour change.[37]

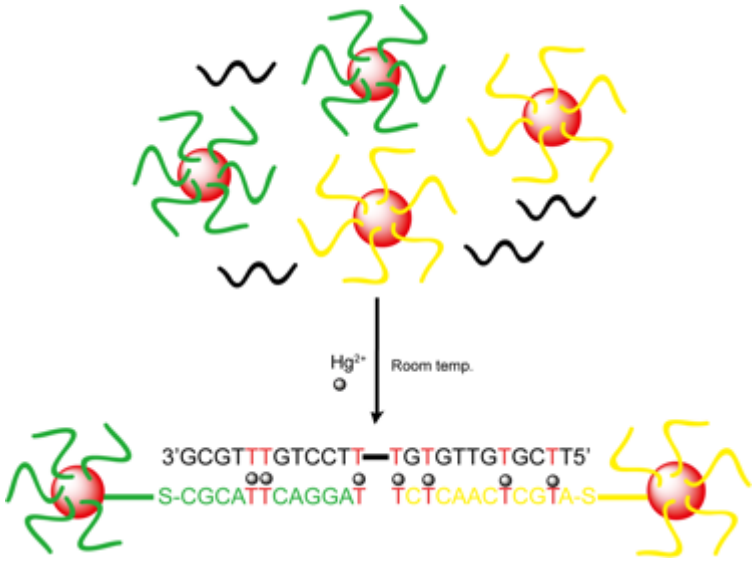

Figure 1. 6 Scheme illustrating the Liu group's colorimetric detection of mercury using DNA-AuNP assays where thymine-Hg^{2+}-thymine complexes formed in the T:T mismatches of linker and AuNP probe strands when mercury was present.

1.4 Responsive disassembly based on DNA displacement

1.4.1 Introduction to DNA displacement

DNA strand displacement is the process of adding an extra DNA strand into a DNA complex made of at least two strands and then the extra DNA replacing one of the hybridized strands to

build a new complex. On the basis of DNA displacement, triggers have been developed to control the assembly or disassembly of DNA structures such as DNA tweezers,[38] DNA walkers,[39] and DNA gears.[40] In a DNA box example, a “lock" and “key" was designed to the box, where the DNA box was closed by “locks” (orange and blue) that are duplexes formed by two short strands protruding from the lid and the main box, respectively. Each “lock” has a small toehold where a “key” sequence signal can open the “lock” by strand displacement.[30] The opening and closing was monitored by changes in Forster resonant energy transfer (FRET) of two cynanine dyes (Figure 1.7).

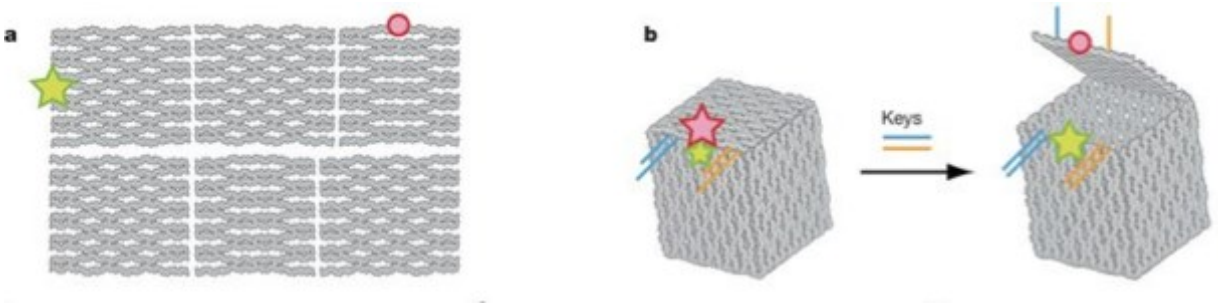

Figure 1. 7 (a) Illustrations of the unlinked sheets functionalized with Cy5 (red) and Cy3 (green). (b) The process of opening of the box lid. The DNA double standed locks are opened by keys leading to the loss of emission of Cy5 by FRET. Imaged adapted with permission from ref. 30. Copyright © 2009, Springer Nature.

1.4.2 Fluorescence detection based on DNA-AuNP structure

DNA displacement has been widely in analytical methods, such as those based on fluorescence and colorimetry, for biomarker detection based on modulation of DNA-AuNP structure. Gold nanoparticles are good fluorescence quenchers because of their high molar absorption coefficient.[41] For instance, the fluorescence of cypate - a near-infrared (NIR) fluorescent dye - was almost completely quenched on the gold nanoparticle surface, and its fluorescence increased

around 17 times at approximately 5 nm from the surface, which is almost the length of 15 nucleotides.[42] In view of that, Dubertret et al. achieved a single mismatch detection by a hairpin DNA-modified AuNP, where the fluorophore was near and quenched by AuNP (Figure 1.8). When the target was present and opened the hairpin structure, the fluorophore went further away from the quencher and fluorescence increased.[43]

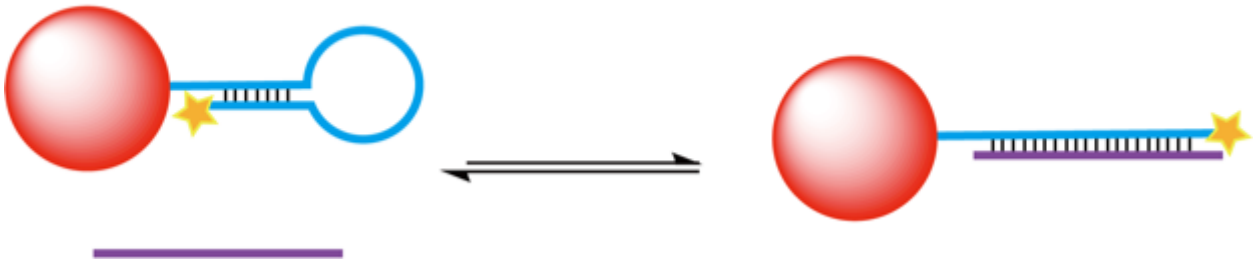

Figure 1. 8 DNA target triggered fluorescence increase from hairpin DNA-AuNPs structure

DNA - gold nanoparticle structures have wide applications in biomarker detection other than DNA.[36] For example, Zhang and coworkers combined multicolour gold nanoprobes for the simultaneous detection of three analytes: adenosine, cocaine, and potassium ion (Figure 1.9).[44] The three DNA sequences conjugated to AuNP were complementary to three DNA aptamers, anti-adenosine aptamer, and anti-cocaine aptamer, and potassium-specific G-quartet aptamer. These three DNA aptamers were labeled with different dyes. When the aptamers hybridized with the strands on the AuNP surface the dyes were quenched by AuNP. Once the small molecule targets

appeared, the aptamers would form the specific conjugations with the small molecules or ions and release the dye-labeled aptamers from the AuNP surface allowing them to be detected.[44]

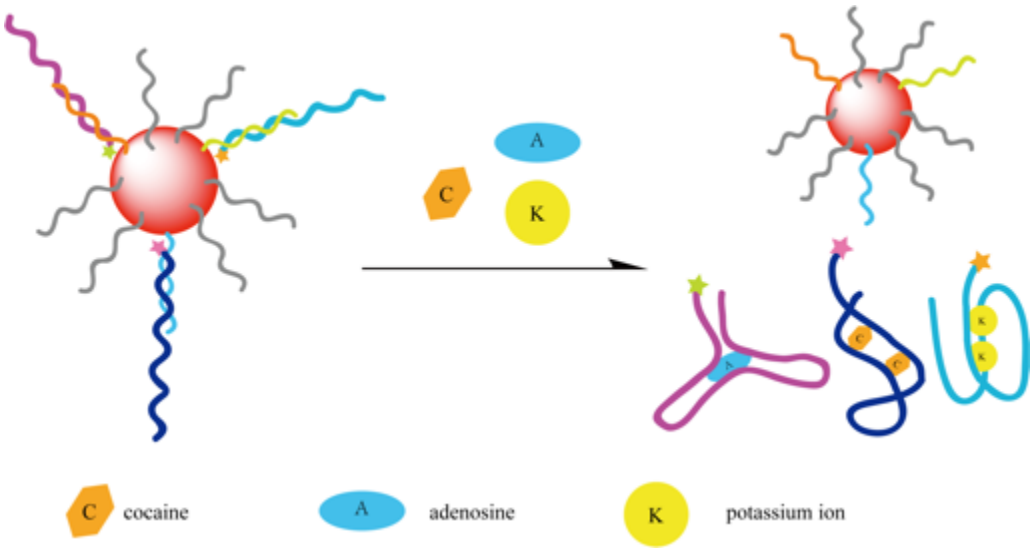

Figure 1. 9 Schematic illustrating simultaneous detection of cocaine, adenosine, and potassium ion. The different DNA aptamer contains different fluorophores. When any target is present, the DNA aptamer would dissociate from gold nanoparticle and emit fluorescence.

1.4.3 - Colorimetric detection based on DNA-AuNPs structure

In addition to fluorescent detection, combining gold nanoparticles with DNA assembly is able to be applied to colorimetric detection of biomarkers. As mentioned, gold nanoparticles have a property that their SPR absorption peak redshifts, leading to a colour change from red to purple, when their diameters are increased[22] or the nanoparticles are aggregated.[23]. Mirkin and coworkers reported two group of AuNPs functionalized by two non-complementary DNA probes respectively. After adding a target strand partly complementary to each probe, the target DNA hybridized with two probes and aggregate gold nanoparticles to resulted in colour change. [34, 45]

However, such target triggered assembly is an intrinsically slow process owing to the repulsive interactions between DNA on the nanoparticles.

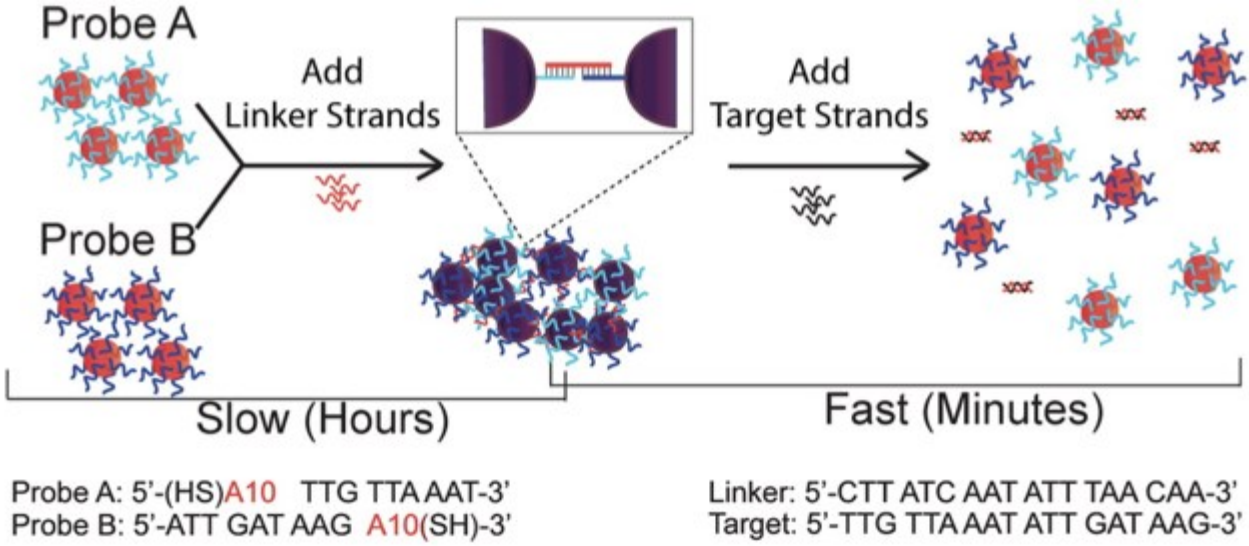

Figure 1. 10 Illustration of aggregates assembly and disassembly. The aggregates formed in several hours after adding the linker strands. However, at a specific temperature target strands added to the aggregates only took 10 minutes to completely disassemble the aggregates. Image reproduced with permission from ref. 46. Copyright © 2016, American Chemical Society

Alternatively, strand displacement/disassembly method can be used in a colorimetric system. In previous work in our lab, Lam et al. prepared DNA-AuNP aggregates with a linker DNA with two respective DNA strands functionalized AuNPs.[46] Following this, the addition of target DNA triggered the disassembly of aggregates via DNA displacement, which only required less than 10 minutes and was therefore much faster than the several hours required for the assembly step (Figure 1.10). Furthermore, toeholds at both 5' and 3' ends of linker allow the target to accomplish a rapid colorimetric detection of 10 pmol DNA target over a wide range of temperatures including room temperature.[47]

Similarly, Xiao et al reported an application for small molecule detection using a DNA-AuNP dimer that dissociated into monomers when triggered by ochratoxin A (OTA),[46] a food-contaminating mycotoxins.[48] In this system, two of the DNA probes were asymmetrically modified on AuNP-1 and AuNP-2, respectively. Another strand, an OTA aptamer, was able to form a Y-shaped DNA duplex by hybridizing the DNA probes (Figure 1.11). OTA would compete with DNA probes to bind the aptamer strand. When OTA was present, the AuNP dimers disassembled and the colour shifted from blue to red.[46]

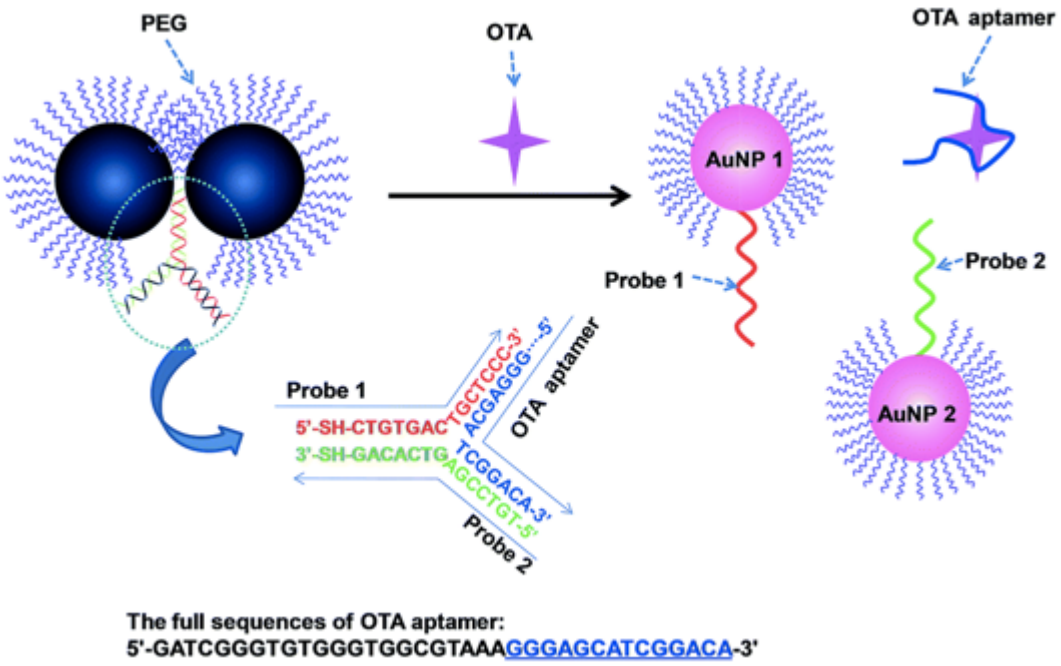

Figure 1. 11 Illustration of the AuNP dimer-based colorimetric sensor. Image reproduced with permission from ref. 46. Copyright © 2015 The Royal Society of Chemistry.

1.4.4 Gold nanoparticle based colorimetric detection with DNA amplification methods

Biomarkers such as specific DNA and RNA in cell samples may be so low as to be undetectable by standard analytical methods. Hence, amplifying the DNA target is a necessary step to increase sensitivity and reduce the detection limit of DNA nanostructures. In 1983, Kary

Mullis developed a method called the polymerase chain reaction (PCR) to generate thousands to millions times more copies of a particular DNA sequence. However, the limitation of PCR is that even the smallest amount of contaminating DNA can be amplified, resulting in misleading or ambiguous results.[49] Also, traditional PCR relies on an instrument that cycles the temperature in every amplification cycle from 48 °C to 95 °C. To simplify the instrumentation required for standard PCR, isothermal amplification methods such as loop mediated DNA amplification (LAMP)[50] and rolling circle amplification (RCA)[51] have been developed.

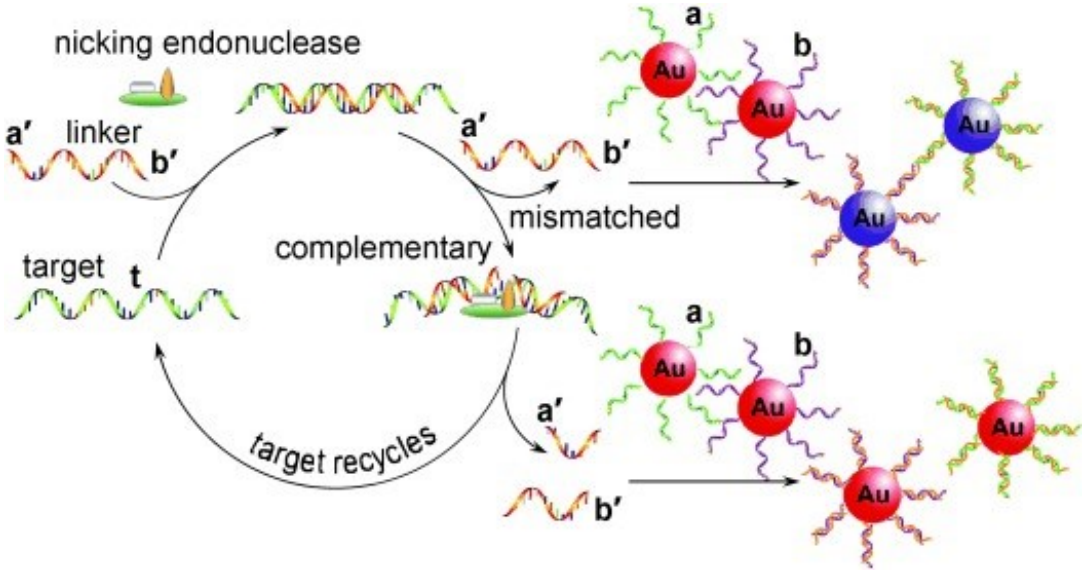

Figure 1. 12 Colorimetric detection of nicking endonuclease assisted nanoparticle amplification (NEANA) method for target DNA. Image reproduced with permission from ref. 52. © WILEY-VCH Verlag GmbH & Co. KGaA, Weinheim

To increase the sensitivity of nanostructures, Xu's group built a nicking endonuclease assisted nanoparticle amplification (NEANA) method for target DNA detection (Figure 1.12). [53] Nicking endonuclease (NEase) only cleaves a DNA duplex rather than a single strand.[54] In this way, they designed a linker DNA which could be cleaved by NEase that was complementary to

the target. When the target was present, the NEase was able to cleave the linker DNA. But if the target was absent, the linker strand was not cleaved. Then they added DNA modified AuNPs into the solution, where two DNA probes were both complementary to the linker. Unreacted linker DNA present in the absence of the target would aggregate gold nanoparticles and make the colour change. In contrast, linker dissociated to two pieces in the presence of the target would not bind the gold nanoparticles to shift the colour. [53]

Another amplification method is hybridization chain reaction (HCR) introduced by Dirks and Pierce in 2004.[55] It has not only PCR-like sensitivity but is also an enzyme-free process. Several groups have combined amplification method with a detection read-out. Liu et al. reported a detection system combining AuNP-based colorimetric detection and HCR amplification as shown in Figure 1.13. [52] They designed two hairpin probes, H1 and H2. Both H1 and H2 included two fragments, where the fragment I (blue part) at H1 was complementary to the fragment I′ (blue part) of H2 and the fragment II (red part) at H1 was complementary to the fragment II′ (red line) of H2. The blue part of fragment I at the 5′ end of H1 was designed to hybridize with the target DNA (green), leading to target strand opening of the H1 hairpin which exposed the fragment II (step 1). Then fragment II of H1 hybridized with the fragment II' of H2 and opens the hairpin to expose fragment I′ (step 2), which was able to hybridize fragment I of H1 (step 3). After several cycles (step 2 and 3), a long double stranded DNA chain was formed, and its negatively charged phosphate backbone was exposed. Unlike, single-stranded DNA that has a high affinity for the Au surface, the long dsDNA weakened the binding with AuNP, so that AuNP aggregated after

addition of salt. And a blue/purple colour variation was observed in the colloid solution when the target was present (Figure 1.13).[52]

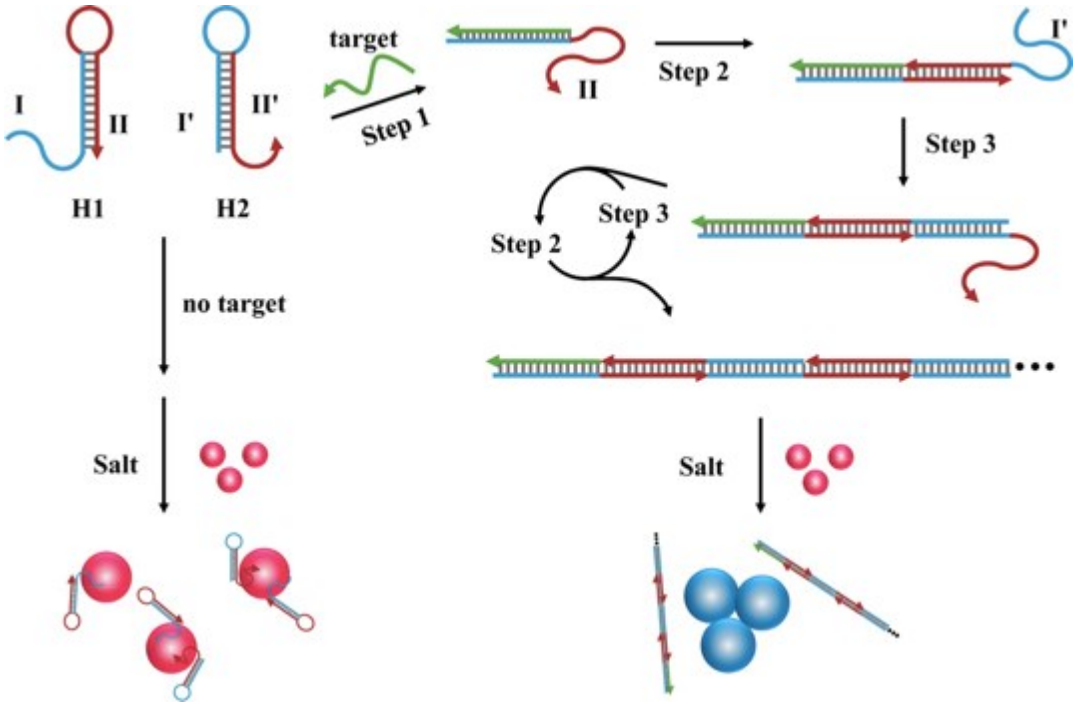

Figure 1. 13 Schematic of combined gold nanoparticle based colorimetric detection and hybridization chain reaction amplification. Image reproduced with permission from ref. 52. Copyright © 2013, American Chemical Society.

Assembly and disassembly based detection schemes of gold nanoparticles have been widely applied for many targets such as small molecules, DNA, protein. The target-triggered disassembly DNA-AuNPs previously explored by our group is a rapid method for DNA detection, but the requirement of target DNA concentration is quite high and it has not been applied in RNA detection based on the disassembly of DNA-AuNPs coupled with an amplification method.

1.5 Responsiveness of different self-assembly systems

Forces involved in molecular self-assembly include Van der Waals interactions,[4] hydrogen bonds,[5] coordination bonds,[6] and π-π stacking,[7] while external modulation of temperature,[56] pH,[57-

[58] light,[59] and fuel[60-61] have also been employed to control the assembly/disassembly of molecules. For example, Yan and coworkers developed a photo-responsive ligand to control hybridization of Anderson-type clusters, an azobenzene modified octahedral structure with a central manganese atom.[59] Another application is pH responsive assemblies. As shown in Figure 1.14, Thamphiwatana et al. designed gold nanoparticles functionalized with chitosan (with a p*K*a ≈ 6), called AuChi.[57] AuChi was deprotonated at neutral pH while its coat was strongly positive at low pH, such as gastric pH.[62] The AuChi were complexed to the surface of liposomes composed of hydrogenated l-α-phosphatidylcholine (egg PC) and 1,2-dioleoyl-*sn*-glycero-3-phosphatidic acid (DOPA); the latter is a phospholipid with a negative charge within the pH range of 1.2–7.4.[63-64] The AuChi was able to tightly bind to the liposome surfaces under low pH (pH=1.2). However, AuChi dissociated from the liposomes once the pH was increased to neutral pH (pH=7.4), which occurred at bacterial membranes of *H. pylori*,[65] , releasing the encapsulated drugs.[57]

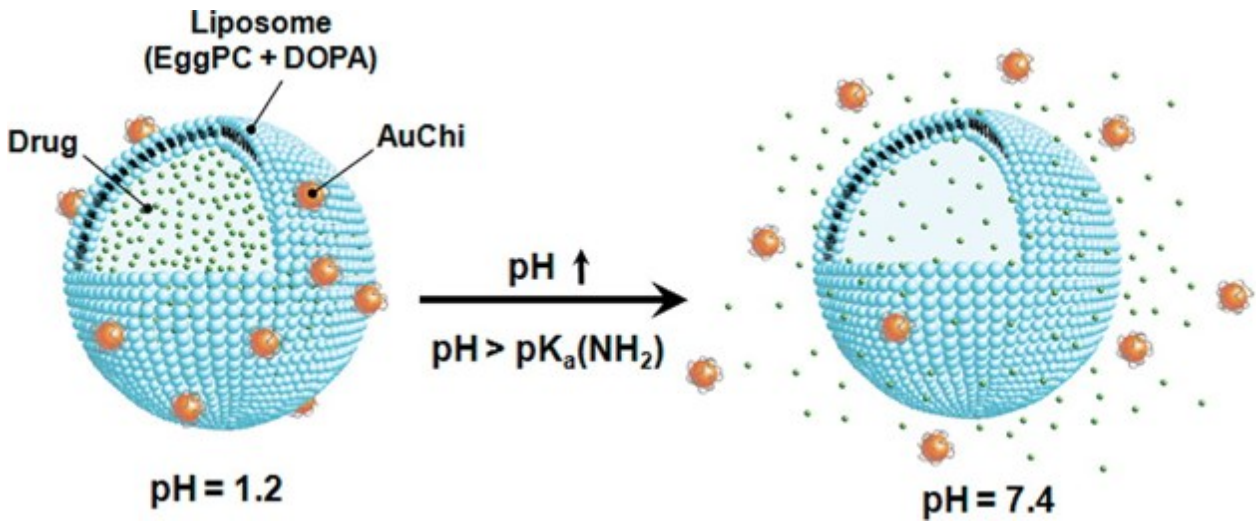

Figure 1. 14 Schematic illustration of pH responsive drug delivery process based on chitosan-modified gold nanoparticles coated phospholipid liposome (AuChi-liposome). the liposome is stabilized by binding of protonated AuChi nanoparticles at gastric pH (pH = 1.2). And AuChi nanoparticles are deprotonated and dissociated from the liposome, resulting in drug release properties at nature pH (pH = 7.4). Image reproduced with permission from ref. 57. Copyright © 2013, American Chemical Society.

An emerging area of interest is in dissipative non-equilibrium assembly of molecules. In these processes an energy source, such as a chemical reactant often referred to as a "fuel", converts the molecule into a less stable form that self assembles.[66] Eventually this molecule will return to its more stable state, and will re-react with the fuel. However, once all of the fuel has been consumed the assemblies dissolve as the molecule returns to its more stable non-assembling state. For example, *N*-(3-dimethylaminopropyl)-*N*′-ethylcarbodiimide (EDC), has also been used to trigger assembly of molecules by activating a carboxylic acid precursor, which is able to undergo self-assembly to form a supramolecular material after the acid is converted to a neutral ester or anhydride.[60] For example, Grötsch et al reported a dissipative self-assembly of silicon

nanocrystals (SiNCs) driven by chemical fuel. The SiNCs were modified by 5-hexenoic acid to make them water-soluble. These particles were dissolved in a buffer at pH 6.5 and combined with 2-(*N*-morpholino) ethanesulfonicacid (MES) and *N*-hydroxysuccinimide (NHS) in water.[61] The pH of 6.5 led > 50% of the carboxylic groups on the SiNCs to be deprotonated. The SiNCs dissolved in the buffer yielded a yellow transparent colloidal solution and emitted red light (luminescence) under UV irradiation (Figure 1.15b). They also determined the size of SiNCs by cryogenic transmission electron microscopy (cryo-TEM) that the diameter was around 3.6 nm (Figure 1.15c). After addition of EDC, the initially transparent solution began to aggregate by self-assembly of the NHS ester product. Once all of the EDC had been consumed, the turbid solution transformed back to yellow clear solution in hours owing to hydrolysis of the NHS esters back to the carboxylic SiNP precursor. The authors found that at least 6.5 mM EDC resulted in a turbid mixture visible by naked eyes (Figure 1.15d). Also the increment of EDC concentration led to longer lived aggregation of the particles[61].

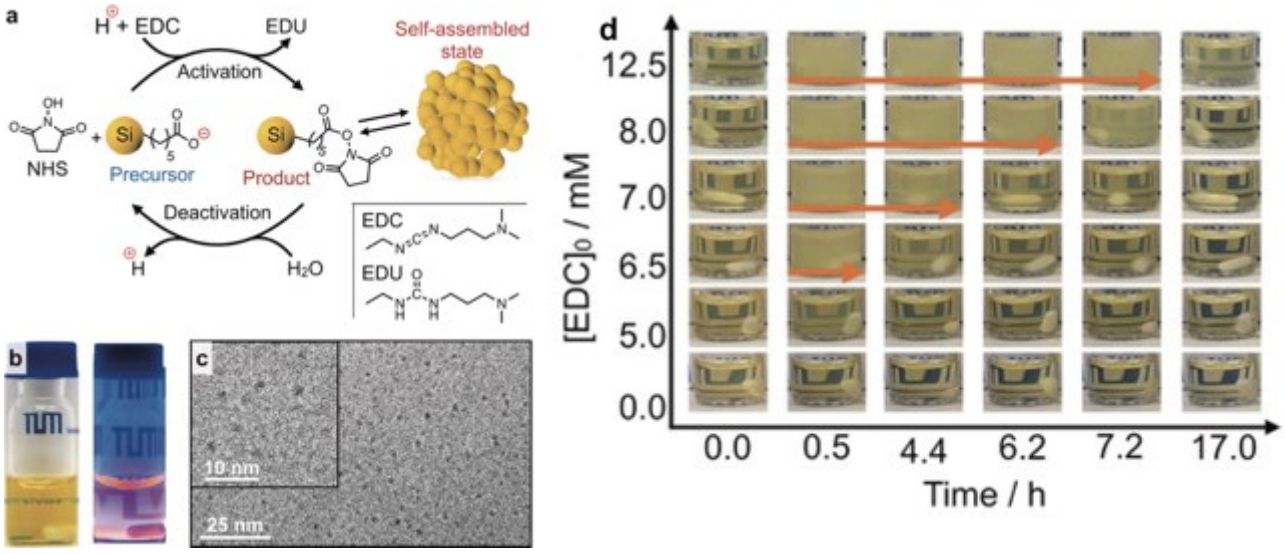

Figure 1. 15 (a) Schematic illustration of fuel-driven self-assembly of SiNCs. Carboxylate groups coated SiNCs were activated by EDC to form an unstable NHS ester. (b) Photographs of precursor solution in MES buffer under visible (left) and UV (365 nm, right) light. (c) Cryo-TEM images of the precursor solution. (d) Photographs of SiNC solutions with different initial EDC concentrations at different time points. Imaged adapted and modified with permission from ref. 61. Copyright © WILEY-VCH Verlag GmbH & Co. KGaA, Weinheim.

The fuel-driven chemical reaction network has also been developed for molecular self assembly into microscopic oil droplets.[61, 67] However, this strategy has not been applied to the assembly of amphipathic molecules into smaller spherical micelles.

1.6 Thesis overview

The world of nanostructure assembly and disassembly is huge and there is certainly room for enhancement. In addition, both assembly and disassembly play significant roles in biology and industrial processes. On the one hand, dissipative self-assemblies have been widely explored from nanoparticles,[61] fibres,[60, 68] supramolecular polymers,[69] and active droplets.[67] However, spherical

micelles formed in response to an energy dissipating chemical reaction cycle has not been reported. On the other hand, colorimetric detection based on DNA disassembly progress using DNA-AuNPs has been widely applied to different biomarkers. Nevertheless, there are few reports of rapid, room temperature, sensitive colorimetric methods for RNA detection.

In Chapter 2, we describe the dissipative self-assembly of amphipathic molecules into spherical micelles at the expense of a chemical fuel. We synthesized an amphipathic molecule by Cu (I)-catalyzed azide/alkyne cycloaddition (CuAAC) reaction. Then we performed kinetic experiments by HPLC to determine the half-life. Using fluorescence spectroscopy to check the emission maximum of Nile red confirmed the self-assembly of the amphipathic molecule by a blue shift from 651 nm to 618 nm after addition of fuel. DLS experiments showed the assembly and dissipation of micelle and cryo-EM illustrated the 3 nm micelles. We demonstrated that we are able to regulate the lifetime of these assemblies by the initial fuel added to the system.

Chapter 3 discusses the colorimetric detection of DNA amplicons generated in a room-temperature amplification process using the rapid disassembly of DNA-gold nanoparticle aggregates also at room temperature. We prepared gold nanoparticle aggregates[46] and found that all four primers of a lesion induced DNA amplification (LIDA)[70-71] would not affect the DNA-triggered disassembly process. Then, we found that 203 fmol target DNA was able to trigger the DNA-gold nanoparticle within 10 minutes after 90-minute amplification at 28 °C. We combined RNA transcription with LIDA and DNA-gold nanoparticles at room temperature to achieve this rapid detection after 90-minute amplification of 1-2 fmol target RNA. Furthermore, the colorimetric detection showed good selectivity that we were able to distinguish the target RNA with single-base mismatch RNA, non-match RNA. Additionally, we successful detected as low as 102 amol of target RNA spiked in 4 μg of human lungs total RNA.

Chapter 2

Dissipative self-assembly of amphipathic molecules into micelles driven by a chemical fuel

2.1 Introduction

The self-assembly of amphipathic molecules plays important roles in both biological and industrial processes.[2, 11, 72] Assemblies of amphipathic molecules have been developed that form a range of structures from spherical[13] and worm-like micelles[14] to bilayers[2] and crystals.[15] These assemblies of amphipathic molecules are found in a broad range of applications like surfactant detergents in soaps, transfection agents, or drug delivery vehicles. More recently, the field has focused on the development of amphiphilic assemblies that are responsive to external stimuli. For example, the use of dynamic covalent chemistry has allowed for the formation of pH-responsive micelles. [73-74]

In dissipative self-assembly, molecular self-assemblies are regulated by the kinetics of a metabolic reaction cycle.[75-77] In the chemical reaction cycle, two reactions are important, the activation reaction which activates molecules for self-assembly at the expense of the irreversible conversion of a chemical fuel, and a deactivation reaction that spontaneously reverts the product to the precursor. Consequently, the assembly is controlled by the kinetics of the chemical reaction cycle, which means that assemblies emerge when fuel is applied, but decay when fuel is running low. Indeed, when a finite amount of fuel is added, the assemblies have a limited lifetime.[78] Dissipative self-assemblies that researchers have explored include fibers,[60, 68, 79] colloids,[80] nanoparticles and microparticles clusters,[61] supramolecular polymers, [69, 81-82] vesicles, [83] and active droplets.[67] However, examples of spherical micelles formed in response to an energy dissipating chemical reaction cycle have not been reported.

The Boekhoven's group recently introduced a chemical reaction cycle that was used to regulate the dissipative self-assembly of fibers at the expense of a chemical fuel.[84] In the reaction cycle, a precursor molecule with two carboxylate groups is converted to its corresponding

anhydride at the expense of a carbodiimide-based condensing agent. Because the reaction cycle operates in water, the anhydride is unstable and rapidly hydrolyzes to the original dicarboxylate precursor. In its limited lifetime, the anhydride can self-assemble. The design strategy to induce self-assembly makes use of the loss of two negatively charged carboxylates upon activation. While the precursor is soluble, the product was designed to self-assemble into fibers, colloids or spherulites.

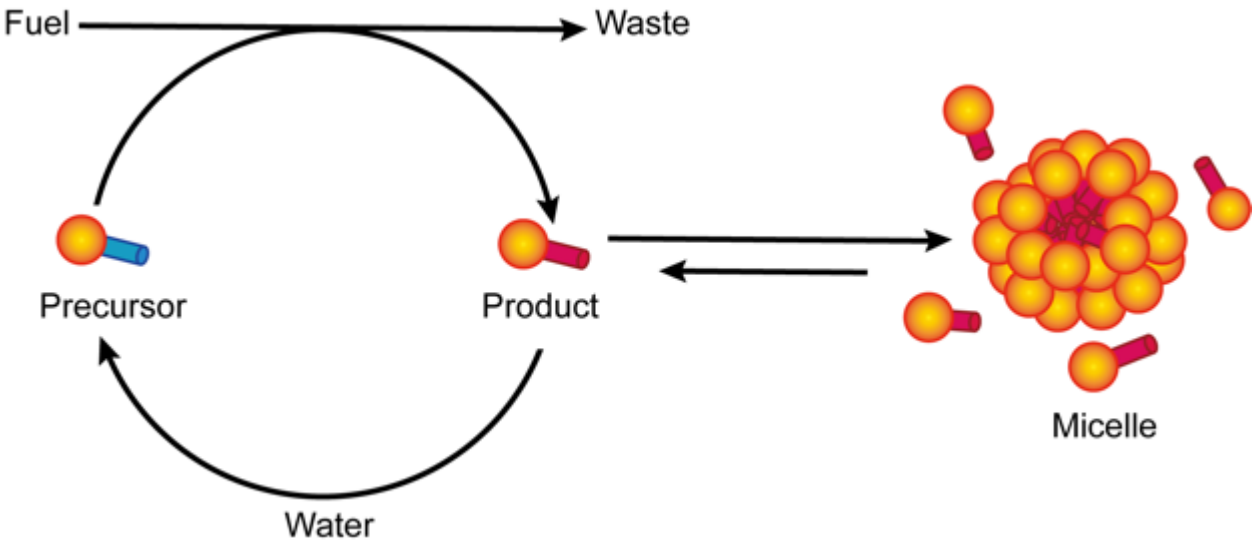

Figure 2. 1 A schematic illustrating self-assembly of micelles driven by a chemical fuel.

Based on this fuel-driven system, we designed an amphipathic molecule to form dissipative spherical micelles. To synthesize this amphipathic molecule, we considered the Cu(I)-catalyzed azide/alkyne cycloaddition (CuAAC), a "click" reaction with high yield could be used as a general strategy to generate a self-assembly. The CuAAC reaction has been widely used in chemical synthesis since 2002, as it is a simple strategy to combine two expected molecular chains together.[85-88] Additionally, Rao et al. used CuAAC reaction to synthesize a Y-shaped polypeptide copolymer that can self-assemble into two different type of micelles at different pH conditions.[74]

In this work, we report the dissipative self-assembly of amphipathic molecules, which are synthesized by a CuAAC reaction, into spherical micelles at the expense of a chemical fuel (Figure

2.1). We demonstrate the emergence of the micelles in response to a chemical fuel, and we show the decay when fuel is depleted. We demonstrate that we can regulate the lifetime of these assemblies by the initial fuel added to the system. Such temporal micelles might prove useful in the development of biomimetic signaling networks or in drug delivery systems.

2.2 Experimental

2.2.1 Compound Synthesis and Purification

All reagents were purchased from Sigma-Aldrich, TCI Chemicals or Alfa-Aesar and used without further purification unless otherwise stated. In Milli-Q water 4-ethynylphthalic anhydride (EPAn) hydrolyzed to 4-ethynylphthalic acid (EPA) in 72 hours. Lyophilizing the reaction solution yielded a white powder, which was used without further purification. A mixture of 49.4 mg (0.26 mmol) 4-ethynylphthalic acid and 53.0 mg (0.28 mmol) 1-azido-2-(2-(2-methoxyethoxy)ethoxy)ethane (TEG(triethylene glycol)-Azide) was dissolved in 9 mL Milli-Q water. The atmosphere in the reaction flask was exchanged to argon (3 minutes argon flow). The catalyst was prepared by mixing 0.5 mL 0.52 mM $CuSO_4$ and 0.5 mL 1.04 mM sodium ascorbate. Then, the catalyst solution (1 mL) was added into the reaction mixture and stirred overnight at room temperature. The crude product was purified by reversed-phase high-performance liquid chromatography (HPLC, Thermofisher Dionex Ultimate 3000, Hypersil Gold 250 x 4.8 mm) in a linear gradient of acetonitrile (ACN, 2% to 98%) and water with 0.1% trifluoroacetic acid (TFA). The lyophilized product 4-(1-(2-(2-(2-methoxyethoxy)ethoxy)ethyl)-1*H*-1,2,3-triazol-4-yl)phthalic acid (Precursor: TEG3-triazolyl-phthalic acid; 76.4 mg, 0.20 mmol, 77.5%) was stored at -20°C. The later was analyzed by NMR, electrospray ionization mass spectrometry in positive mode (ESI-MS, Varian 500 MS LC ion trap spectrometer) and HPLC (Thermofisher Dionex

Ultimate 3000, Hypersil Gold 250 x 4.8 mm) eluted with a gradient of 0.1% TFA in water: ACN from 98:2 to 2:98 in 10 min).

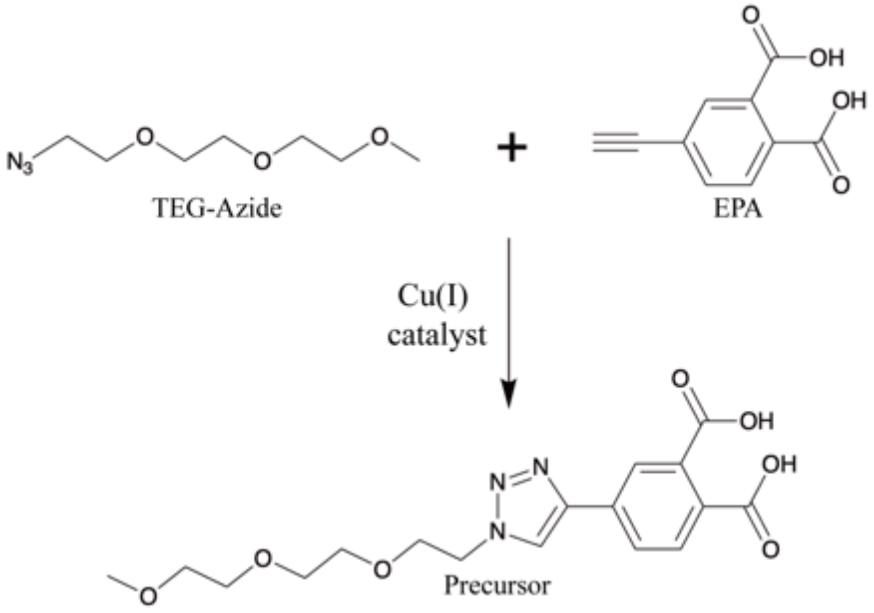

Figure 2. 2 Scheme of synthesis of 4-(1-(2-(2-(2-methoxyethoxy)ethoxy)ethyl)-1*H*-1,2,3-triazol-4-yl)phthalic acid

Characterization of 4-(1-(2-(2-(2-methoxyethoxy)ethoxy)ethyl)-1H-1,2,3-triazol-4-yl)phthalic acid:

Yield 77.5% ^{1}H NMR: (300 MHz, Deuterium Oxide) δ 8.20 (s, C*H* triazole, 1H), 7.82 (d, CH Benzene, 1H), 7.71 (dd, CH Benzene, 1H), 7.63 (d, CH Benzene, 1H), 4.51 (t, CH_2-triazole, 2H), 3.85 (t, OCH_2 2H), 3.62 – 3.47 (m, OCH_2CH_2, 3H), 3.51 – 3.20 (m, OCH_2CH_2, 7H), 3.05 (s, CH_3, 3H). ESI-MS: Calculated: ($C_{17}H_{23}N_3O_7$) m/z = 379.37; Observed: m/z = 380.10, $[Mw+H]^+$. Retention time: 7.56 minutes (Thermofisher Dionex Ultimate 3000, Hypersil Gold 250 x 4.8 mm, eluted with a gradient of 0.1% TFA in water: ACN from 98:2 to 2:98 in 10 min).

2.2.2 Anhydride preparation

For a 20 mM stock solution 39.77 mg TEG-triazolyl-phtalic acid precursor was dissolved in 5 mL 0.2 M 2-(N-Morpholino)ethanesulfonic acid (MES) buffer. Afterwards, the pH was adjusted to 6.0 and the solution filtered by a 0.2 µm syringe filter. For each fuel experiment a new stock solution of *N*-(3-Dimethylaminopropyl)-*N'*-ethylcarbodiimide (EDC) was prepared by dissolving EDC hydrochloride (CAS # 25952-53-8) powder in Milli-Q water. The reaction cycle was initiated by the addition of the EDC stock solution to the precursor solution (Figure 2.3). In the activation reaction, the carboxylate groups of precursor were converted into anhydride by the irreversible consumption of EDC. In the deactivation reaction, the anhydride hydrolyzed back to initial carboxylate format. Once EDC was depleted, the activation step would terminated.

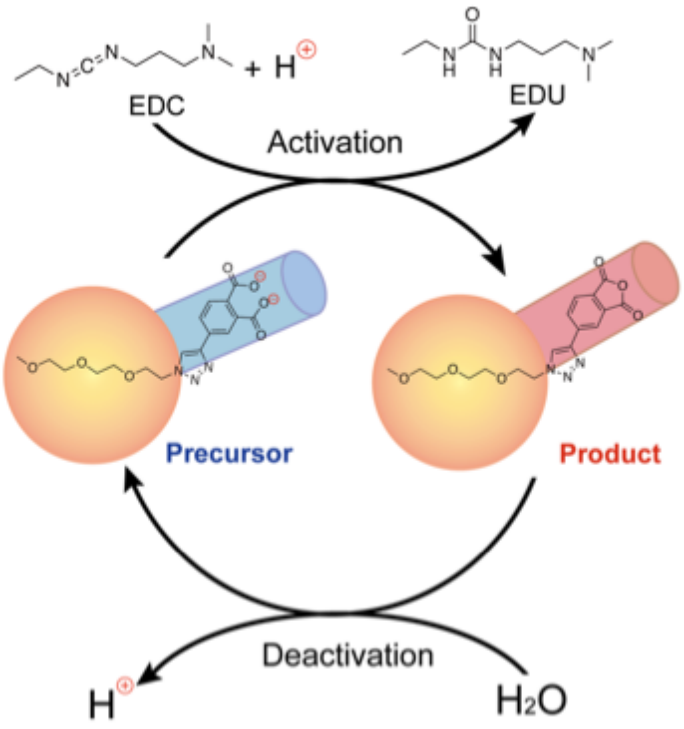

Figure 2. 3 Schematic cycle of fuel-driven reaction. Carboxylate groups react with EDC to anhydride and then come back to carboxylate structure by hydrolysis.

Characterization of 4-(1-(2-(2-(2-methoxyethoxy)ethoxy)ethyl)-1H-1,2,3-triazol-4-yl)phthalic anhydride:

Triethylene glyocol (TEG)-triazolyl-phthalic anhydride was formed by addition of 50 µL 4 M into 500 µL 20 mM TEG-triazolyl-phthalic acid and was analyzed immediately by LC-MS. The compound was also analyzed by HPLC with a gradient of 0.1% TFA in water: ACN from 98:2 to 2:98 in 10 min. This anhydride (TEG-triazolyl-phthalic anhydride) is hard to purify in small amount, because it decays fast in water/ACN gradient of HPLC. Therefore, this molecule is diffcult to identify by NMR. ESI-MS: Calculated: ($C_{17}H_{21}N_3O_6$) m/z = 361.35; Observed: m/z = 362.16, $[Mw+H]^+$. Retention time: 9.45 minutes (Thermofisher Dionex Ultimate 3000, Hypersil Gold 250 x 4.8 mmeluted with a gradient of 0.1% TFA in water: ACN from 98:2 to 2:98 in 10 min).

2.2.3 Kinetic model

The kinetics of the reaction was monitored over time by means of analytical HPLC. A 500 µL TEG-triazolyl-phtalic acid precursor solution after addition of EDC was prepared as described above and placed into a screw cap HPLC vial without. Every 15 minutes, 1 µL of the solutions in the vial was injected into HPLC, and separated by a linear gradient water : ACN from 98:2 to 2:98 in 10 minutes (other 5 minutes: clean and come back to 98:2). Calibration curves for the precursor (λ= 254 nm) were performed in triplicate in order to quantify the compounds over time. Absorption coefficient of fuel (λ= 220 nm) was provided by Boekhoven's group, which is 0.2511 mAU·min/mM for 10 µL injection. However, calibration was not possible for the anhydride due to the instability in water. Instead, the same absorption coefficient as their corresponding precursor was used. Measurements were operated at 25 ºC.

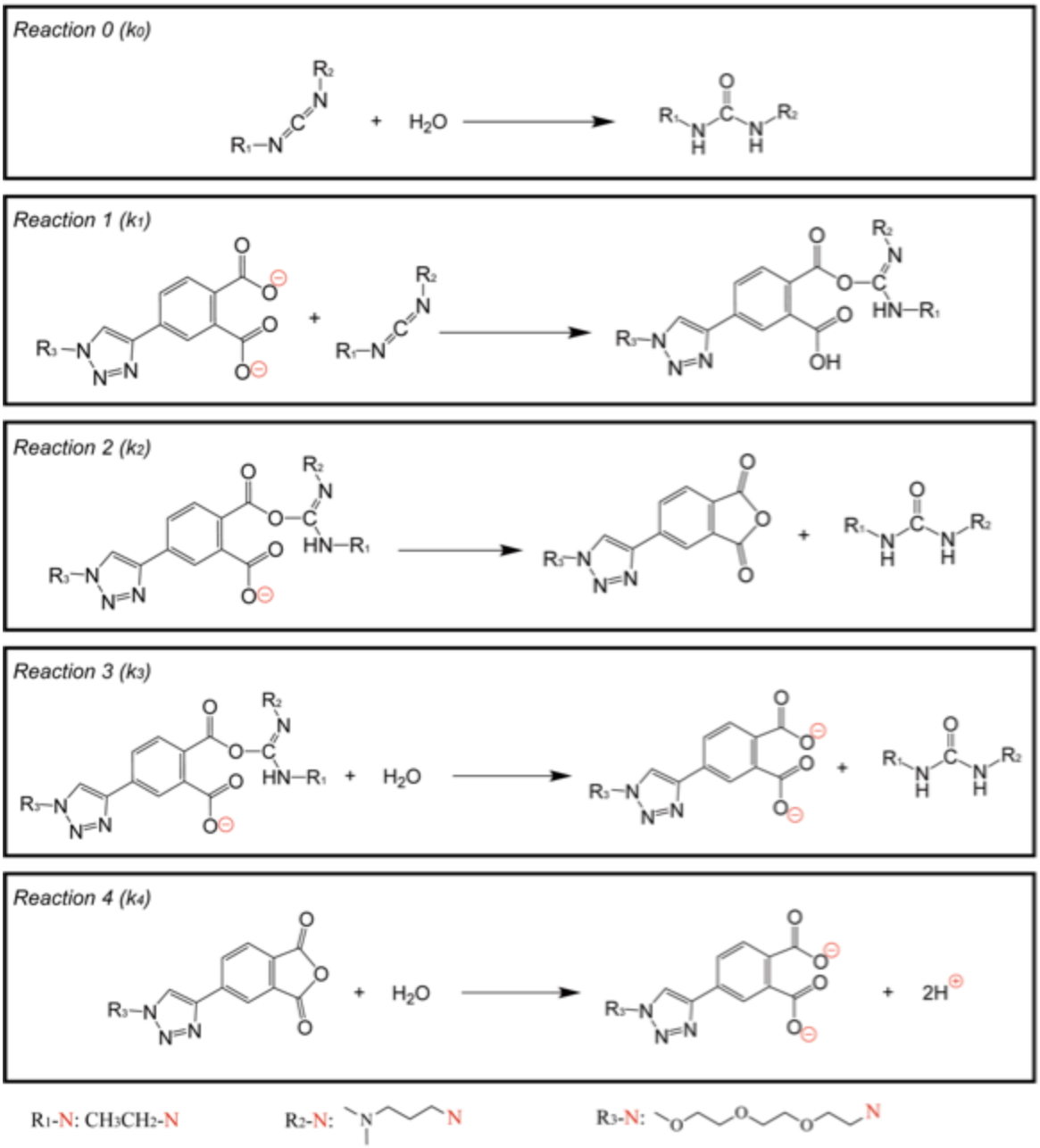

Figure 2. 4 Scheme of each steps of reaction.

A kinetic model was written using Matlab in which the reactions above were described. The concentrations of each reactant were calculated for every 1 second in the cycle.

Reaction 0 (k_0) is the direct hydrolysis of carbodiimide with a first order rate constant of 1.3×10^{-5} sec^{-1} as determined by HPLC (provided by Boekhoven's group) and implies that in most

experiments at pH = 6.0 in 0.2 M MES buffer. This constant is closed to the research by Gilles et al., where they showed the hydrolysis of EDC is a pseudo-first-order process, depended on pH value, and the kinetic constant was around 0.96 x10-5 sec-1 at pH 6.0.[89]

Reaction 1 (k_1) is the formation of O-acyl urea by reaction with and EDC. This second order rate constant was dependent on the concentration of the precursor. The rate constant was determined for each precursor by HPLC, by monitoring the EDC consumption.

Reaction 2 (k_2) is the formation of anhydride from O-acyl urea with a first order rate constant and *Reaction 3 (k_3)* is the direct hydrolysis of O-acyl urea. Both rate constants could not be determined because the O-acyl urea was never observed. Those were set to be several times of the rate of k_1. For example, Tena-Solsona et al. set k_2 as twice of k_1 and k_3 as 2.5 times of k_1 using Matlab model.[84] Based on previous work, the O-acyl urea did not reach concentrations over 1 μM in the model.[67, 84]

Reaction 4 (k_4) is the hydrolysis of anhydride with a (pseudo)-first order rate as determined by HPLC. Additionally, this constant can be used to determine the half-life of dissipative amphipathic molecules.

This amount of unwanted reaction such as N-Acyl urea was never greater than 2% of the amount of EDC.

Therefore, each of reaction rate at *time = i (s)* is able to be described as:

$$r_0(i) = k_0 \times [EDC(i)];$$
$$r_1(i) = k_1 \times [EDC(i)] \times [COOH(i)];$$
$$r_2(i) = k_2 \times [COOEDC(i)];$$
$$r_3(i) = k_3 \times [COOEDC(i)];$$
$$r_4(i) = k_4 \times [COOOC(i)].$$

COOH: precursor; COOEDC: O-acyl urea; COOOC: Anhydride.

Then according to the reactions, the concentration at $i+1$ second can be written as:

$$[EDC(i+1)] = [EDC(i)] - r_1(i) - r_0(i);$$
$$[COOH(i+1)] = [COOH(i)] - r_1(i) - r_2(i) + 2r_4(i) + r_3(i);$$
$$[COOEDC(i+1)] = [COOEDC(i)] + r_1(i) - r_2(i) - r_3(i);$$
$$[COOOC(i+1)] = [COOOC(i)] + r_2(i) - r_4(i);$$
$$[EDU(i+1)] = EDU(i) + r_2(i) + r_0(i) + r_3(i).$$

Calibration curve for precursor was determined by measuring HPLC peak area of different concentration precursors provided the coefficient of the ratio of EDC peak area (λ= 254 nm) to EDC concentraion is 9.5265 mAU·min/mM for 1 µL injection (Figure 2.5a). Peak areas of EDC and anhydride of each kinetic reaction were measured and then converted to concentrations. The curves of EDC and anhydride were simulated using Matlab by changing kinetic constants.

Table 2. 1 Preparation of varying concentration of EDC in 20 mM Precursor

nominal [EDC]	Stock EDC	V_{pre} [µL]	real [EDC]	Vol % (EDC to V_{pre})	error
50 mM	12.5 µL (2 M)	500	48.8 mM	2.5%	2.4%
75 mM	18.75 µL (2 M)	500	72.3 mM	3.75%	3.6%
80 mM	20 µL (2 M)	500	76.9 mM	4%	3.8%
100 mM	12.5 µL (4 M)	500	97.6 mM	2.5%	2.4%
150 mM	18.75 µL (4 M)	500	144.6 mM	3.75%	3.6%
200 mM	25 µL (4 M)	500	190.5 mM	5%	4.75%
500 mM	62.5 µL (4 M)	500	444.4 mM	12.5%	11.1%*

The 2 M and 4 M EDC solution was freshly prepared before each experiment. The appropriate volume of stock EDC as per table 2.1 was pipetted into 500 µL of 20 mM precursor solution. Previous work on a similar chemical network reaction[66, 83] used a maximum EDC nominal concentration of 200 mM ± 5%. The MES buffer used was 200 mM and the EDC solution was prepared with EDC hydrochloride. 500 mM EDC solution had more than 10 % error but the

concentration is higher than buffer. Therefore, 500 mM results were considered as a reference of high fuel concentration.

2.3 Results and Discussion

2.3.1 Kinetic analysis of reaction cycle based on anhydride formation

Figure 2.5a shows the calibration curve of the TEG-triazolyl-phthalic acid based on the peak areas in the HPLC separation. Using this calibration curve, we determined the concentration of anhydride as a function of time for reactions consisting of different initial concentrations of acid precursor at 20 mM concentration of EDC (Figure 2.5b and c). We then used the kinetic model described previously to fit to the data. This was achieved by varying each of the four rate constants manually until the best fit to the eye was achieved.

When setting the four constants as k_1 = 0.30 mM·s^{-1}, k_2 = 1.20 s^{-1}, k_3 = 0.75 s^{-1}, k_4 = 0.017 s^{-1}, the simulating curves roughly matched the experimental results (Figure 2.5). Hence, the half-life of amphipathic anhydride molecules dissipation is found to be 40 seconds based on the value of k_4. The experimental results (dots) fit the simulated curves when the EDC concentration was smaller than 100 mM. However, when the concentration of the fuel was more than 100 mM, the experimental results cannot match the simulation any more, especially the 500 mM. The possible reason would be pH change of the buffer.

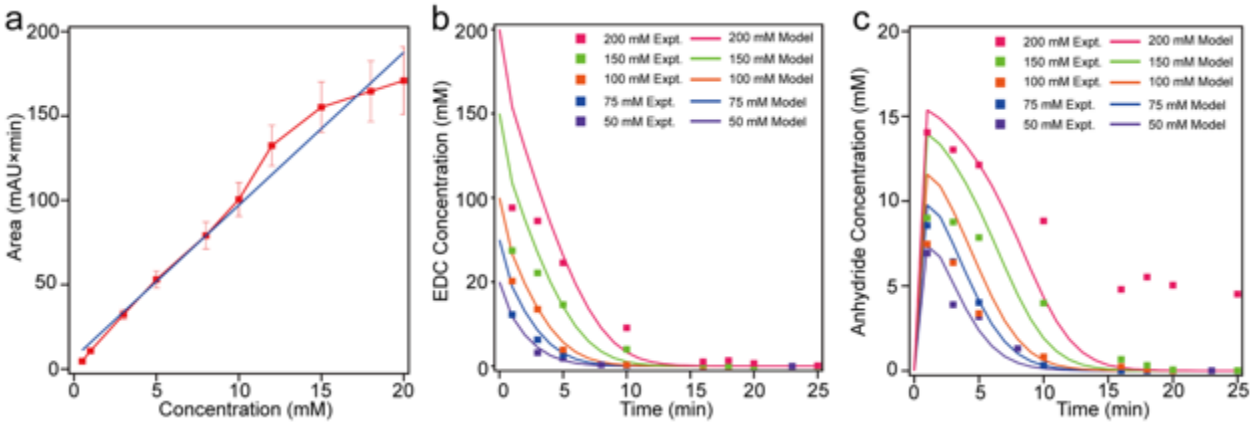

Figure 2. 5 Kinetic experiments of fuel-driven assembly. a) Calibration and fitting curves of precursor phthalic acid. EDC concentration (b) and anhydride concentration (c) against time for 20 mM precursor adding different concentrations (line: simulating result, square: experimental result; purple: 50 mM, blue: 75 mM, orange: 100 mM, green: 150 mM, pink: 200 mM of EDC).

2.3.2 Monitoring self assembly kinetics using fluorescence

As mentioned earlier, the amphipathic molecules form micelles driven by its hydrophobic interaction. This process of the hydrophobic chain could be detected by fluorescence spectroscopy using the solvatochromic probe Nile red (NR), where the maximum emission wavelength (λmax) showed a significant blue shift.[16, 88-89] Therefore, in the experiment, 1 µL of 2.5 µM Nile red in methanol was pipetted into 500 µL of 20 mM precursor solution in a polystyrene cuvette. Then, EDC solution was added into the cuvette, and analysis was started rapidly using a fluorescence spectroscopy, Jasco (JascoFP-8300) spectrofluorometer with an external temperature control (Jasco MCB-100) set at 25 ºC. In the presence of more than 100 mM EDC, the emission intensity of NR showed a significant increase together with a blue shift of the λmax from 651nm to 618 nm. Interestingly, the λmax did not red shift back to initial 651 nm after decaying of the EDC. It might be due to the urea derivative EDU (1-(3-dimethylaminopropyl)-3-ethyl urea). Indeed, in a control experiment having 200 mM EDU, it showed about 5 nm blue shift (Figure 2.6a). The blue shift of λmax of NR with precursor disappeared at around 5.5 min, which is corresponding to around 5

mM. This result showed that its critical micelle concentration (CMC) is around 5 mM. In literature, it was reported that the CMC for tetraethylene glycol monooctyl ether (C8E4) which is a similar amphipathic molecule with similar hydrophilic chain, was 8.4 mM. This value is close to the value of precursor,[89] suggesting that the fuel is able to trigger the assembly of the dissipative micelle.

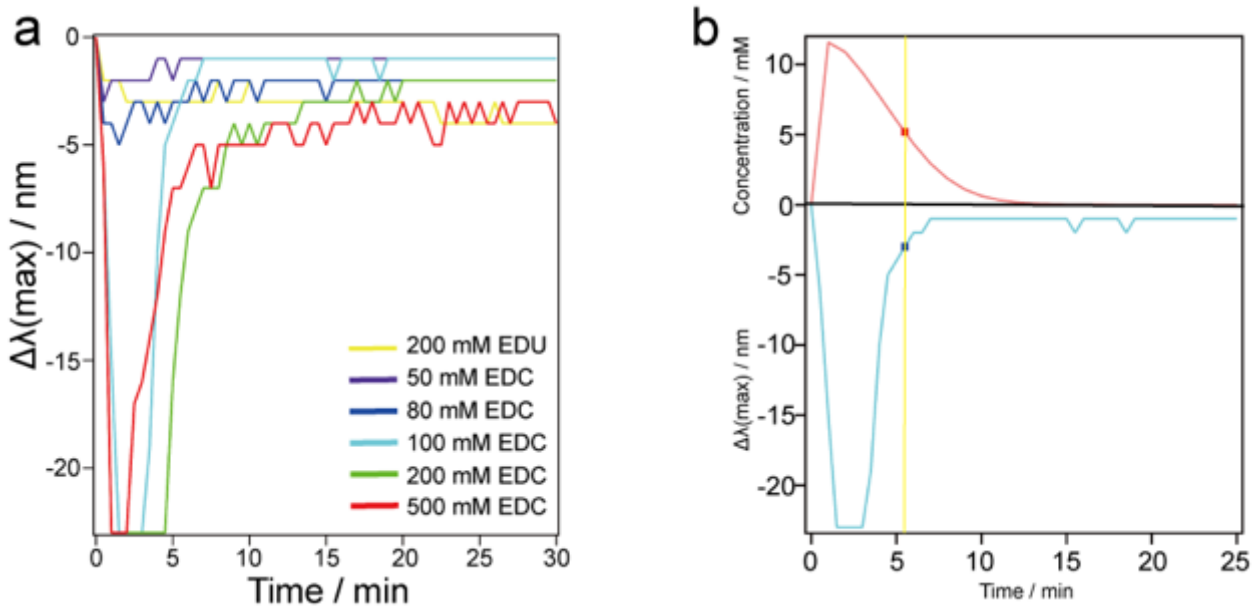

Figure 2. 6 (a) The blue shift of λ_{max} of Nile red with precursor after addition of EDC. (b) Matlab simulation (red) and experiment (blue) of 100 mM EDC with 20 mM precursor. The micelle decayed in 5.5 min (blue square) and the corresponding critical micelle concentration is around 5 mM. Experimental conditions: 20 mM percursor, 5 nM Nile red with different concentration of EDC, 25 °C.

2.3.3 Monitoring self assembly kinetics using fluorescence by dynamic light scattering

Dynamic light scattering (DLS) is a non-invasive technique to determine changes in size of small particles, proteins, polysaccharides, and supramolecular assemblies.[90] To further confirm the assembly of micelle, DLS measurements were performed using a Malvern Zetasizer Nano ZS with

a laser wavelength of 618 nm corresponding to that of Nile red with micelle. Each measurement consisted of 11 acquisitions with an acquisition time of 30 s. 500 µL of 20 µM stock precursor solution in 1 µL of 2.5 µM Nile red solution in a disposable polystyrene cuvettes was used as blank. Then various concentrations of stock EDC solution was used into different cuvette to do the experiment. Each experiment was done in triplicate. Similar to the previous experiement, we used EDU as a control experiment to eliminate the effection of urea derivative.

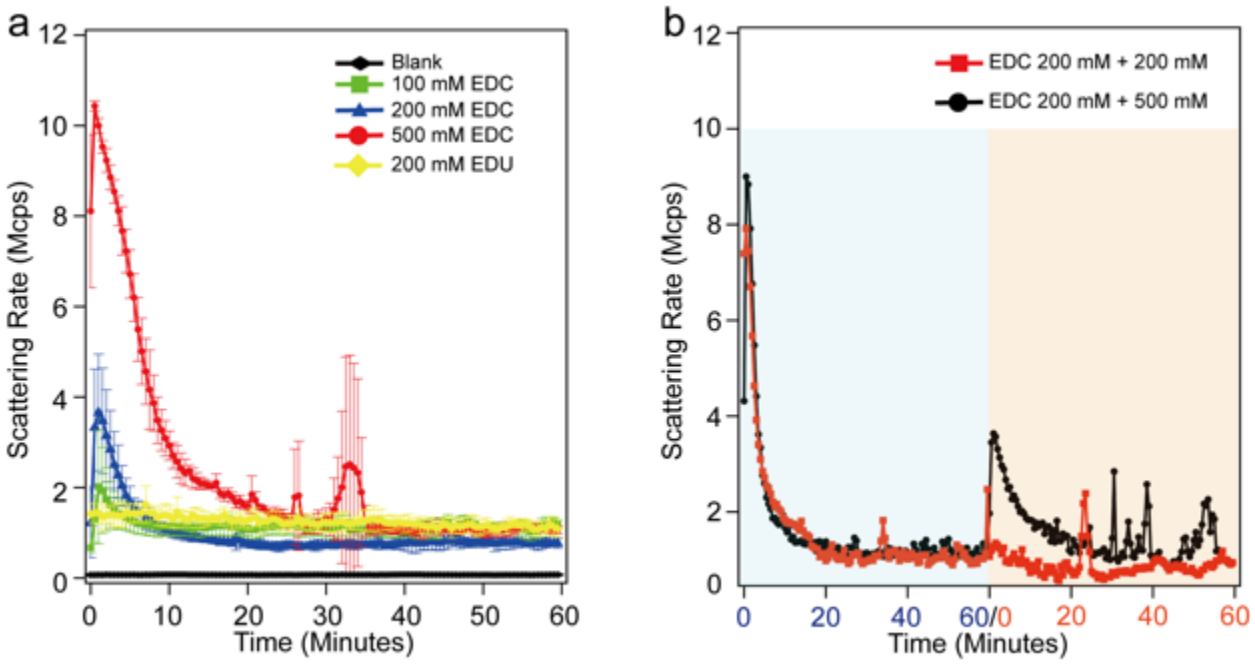

Figure 2. 7 (a) DLS scattering intensity against time for 20 mM precursor with varying concentration of EDC, namely 0 mM (blank), 100 mM, 200 mM, and 500 mM, and control experiment with 200 mM EDC. (b) Cycle experiments that the second addition of EDC was measured after 2 hours of the first addition with 200 mM EDC.

As shown in Figure 2.7a (green trace), 100 mM EDC triggered the assembly of micelles or aggregates followed by micelles disassembly within 10 minutes. 200 mM (blue trace) and 500 mM (red trace) EDC experiments showed a higher scattering rates and longer dissipative time.

Similarly with the emission maximum, the scattering rates did not return to the blank level when the fuel was consumed. The reason might be the formation of EDU which is be affecting the assembly of micelles and this was confirmed by the control experiment shown in Figure 2.7a, yellow trace. To check the sustainability of precursor, the above experiment was repeated with the exception that EDC was added in two rounds. 200 mM of EDC was added in the first round and then 200mM or 500mM of EDC was added again in the second round after 1 hour as shown in Figure 2.7b red trace and black trace respectively. Unfortunately, having same concentration of EDC as same as first round could not achieve a new micelle assembly (red trace). However, with the second round of a higher concentration (500 mM) of EDC, assembly was observed after 2 hours of the first addition (black race). The limitation of DLS experiment is that it did not show the exact size of the micelle that the results was in micrometer scale, which is larger than exception.

2.3.4 Cryogenic-transmission electron microscopy for measuring the size of micelle

To investigate the size of micelle, cryogenic- transmission electron microscopy (Cryo-EM) was used. The instrument was operated by Caren Wanzke and the Cryo-EM images was generated on a JEOL JEM-1400 microscope operating at 120 kV. The images were recorded in a low-dose mode on a CCD camera. Quantifoil R2/2 on copper grid 400 mesh were used. The grids were freshly glow-discharged for 30 seconds prior to use. Preparation of the grids was performed in a FEI Vitrobot at 21 °C with the relative humidity set to 100% and the blotting force was set to -5.

The micelle solution was prepared by adding 12.5 μL of 4M EDC stock solution to 100 μL of 20 mM precursor solution. The 5 μL of mixture sample was incubated at room temperature for 3 minutes, blotted twice for 3.5 seconds and then directly plunged into liquid ethane that was pre-cooled by liquid nitrogen. The cryo-EM grids were transferred and stored in liquid nitrogen, and when needed, placed into a Gatan 625 cryo-specimen holder to insert into the microscope. The

specimen temperature was maintained at -170 °C during the data collection. Figure 2.8 shows the Cryo-TEM image where each black spot represents a micelle. The size of the micelles were found to be around 2.10 ± 0.36 , which supported the micelle formation.

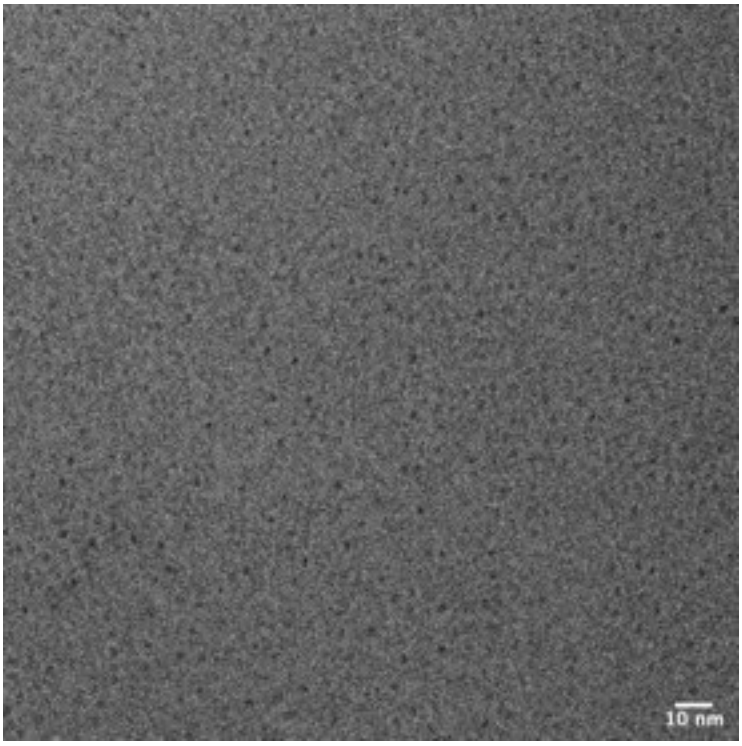

Figure 2. 8 Cryogenic-transmission electron microscopy of 500 mM EDC combined with 20 mM precursor after 3 min. *Scale bar, 10 nm*.

2.4 Conclusion

In this work, we have developed a new strategy to synthesize the dissipative amphipathic molecules by CuAAC click reaction. This amphipathic molecules was able to self-assembly to spherical micelles consuming a chemical fuel such as EDC. Based on the kinetic experiments, we determined that the half-life of this amphipathic molecule in water was 40 seconds. The emission maximum of Nile red with amphipathic molecule showed a blue shift of the λ_{max} from 651nm to

618 nm upon addition of fuel. DLS experiments further proved the assembly and dissipation of the micelles. However, it did not show the size of micelles. With Cryo-EM, the size of the micelles was found to be 3 nm micelle upon fuel addition. In all the experiments performed, we showed only one example of CuAAC click reaction applied to dissipative amphipathic molecules. There a probably concern is the structure of the micelle. In the future, we will use NMR to comfirm the micelle structure and critical micelle concentration. [91] Furthermore, we plan to analyze more molecules and expand this chemical reaction network. Also, we need to compare this dissipative amphipathic molecule with other similar molecules, such as di(ethylene glycol) benzyl ether, to discover the differences.

Chapter 3

Colorimetric detection of DNA amplicons using the rapid disassembly of DNA-gold nanoparticle aggregates at room temperature

3.1 Introduction

Gold nanoparticle assembly systems have been applied to detection of targets such as oligonucleotides,[92-93] proteins[94-95] and metal ions.[96-98] The ability of gold nanoparticles to conjugate with recognition agents such as nucleic acids plays a significant role in assembling sensors.[99] Ribonucleic acid (RNA) as a biomarker has been used in the diagnosis of a range of diseases over the last few decades.[100-101] Many infectious viruses such as HIV, Ebola, Zika have RNA as their genetic material rather than DNA.[102] In addition, microRNA (miRNA) is a class of naturally occurring RNA (19-23 nucleotides), which is widely found in various diseases such as cancers.[50] Therefore, the development of a simple, rapid and sensitive RNA detection sensor that can be used for early disease diagnosis in developing countries where infectious diseases are more prevalent.

Our group has developed a rapid colorimetric detection method based on the disassembly of aggregated DNA-modified gold nanoparticles, which can operate over a wide range of temperatures.[103] The gold nanoparticle aggregates are formed over hours through DNA hybridization of DNA bound to the nanoparticles with a linker DNA in solution. However, upon adding target DNA that is complementary to this linker, disassembly is accomplished within 10 minutes. Moreover, by adding a nucleotide overhang region on the both sides of the linker, we were able to perform colorimetric detection at room temperature.

One major problem of nucleic acid based diagnostics is the low concentration of nucleic acid biomarker in the biological sample, such as blood, urine or saliva.[50, 104] Amplification methods like polymerase chain reaction (PCR) are able to generate hundreds of times more copies of that particular DNA sequence.[49] Similarly, isothermal amplification methods such as loop mediated DNA amplification (LAMP)[50] and rolling circle amplification (RCA)[51] have been developed. I collaborated with my colleague B. Safeenaz Alladin-Mustan to combine this approach with our

group's DNA amplification technique that works at one temperature: lesion induced DNA amplification (LIDA).[70-71] LIDA has proven to be a general method for DNA amplification of short DNA sequences.[70] Previous work has shown that LIDA can be performed over a wide range of temperatures that constitute room temperature and on the benchtop without any equipment besides pipettes and eppendorf tubes.[71]

We are now expanding LIDA to the detection of RNA biomarkers. For the latter, the first step consists of transcribing the RNA to complementary DNA (cDNA), which can then be amplified and detected using LIDA. The set up of the experiment consists of only two tubes (with and without the target RNA) with the required reagents (15 μL total volume) on a tube rack placed on the bench top at room temperature. Then, the resulting DNA amplicons can be detected colorimetrically also at room temperature by adding them to DNA-modified gold nanoparticle aggregates.

With this combination we achieved rapid, isothermal RNA triggered DNA amplification on the bench top without heating equipment. Additionally, we reduced the limit of detection (LOD) for this colorimetric detection method by combining it with our amplification technique.

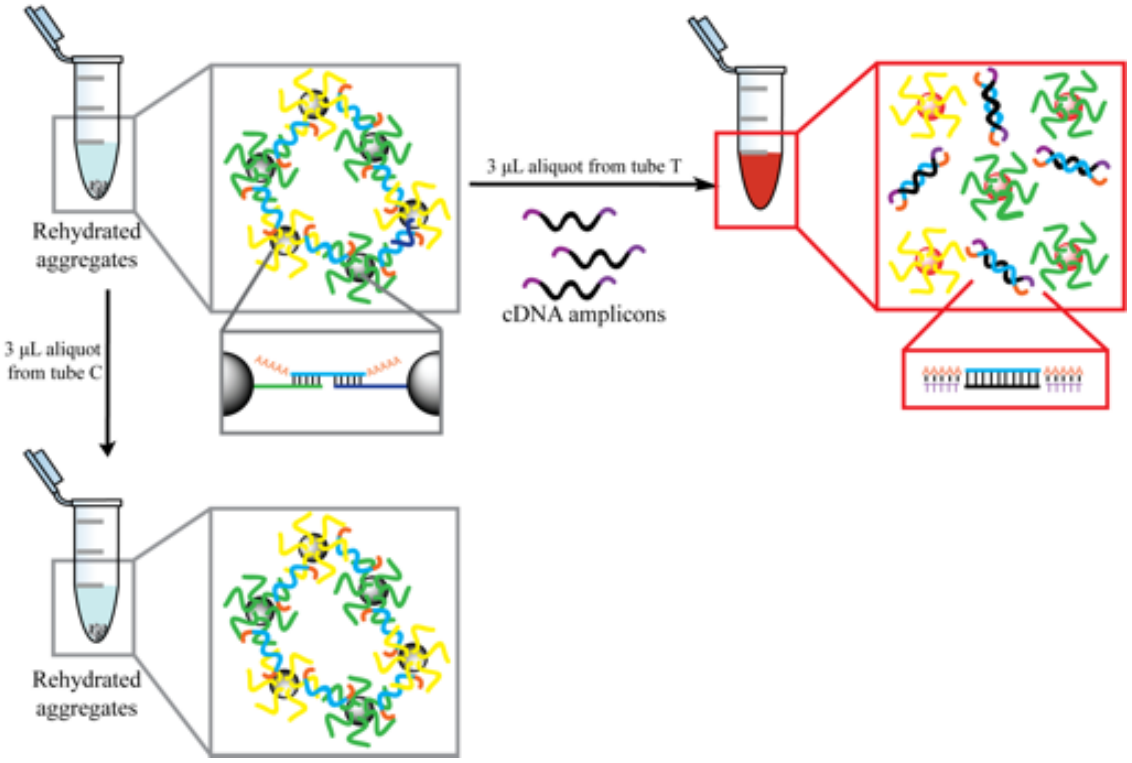

Figure 3. 1 Schematic illustrating DNA-gold nanoparticle conjugation. Aggregates were hybridized by a linker strand. Upon the addition of an aliquot of the amplification solution after the appropriate amount of time, the target amplicons bind the linker strand and release AuNP on the order of minutes.

3.2 Experimental

3.2.1 Oligonucleotides

All RNA oligonucleotides were purchased from Integrated DNA Technologies (IDT, Iowa, USA). All DNA oligonucleotides were synthesized by Applied Biosystems Model 392 DNA/RNA Synthesizer on DMT-ON model using reagents from Glen Research (Sterling, VA). All synthesized DNA was deprotected by NH_4OH and then purified with the DMT-On protocol by using Glen-Pak cartridges (Glen research, Sterling, VA) following the manufacturer's instruction. The strands were characterized by MALDI-TOF under a linear negative mode using a Voyager

Elite time of flight-mass spectrometer (Applied Biosystems, Foster City, CA).[105] Purity was assessed by visualizing the oligonucleotides with StainsAll reagent (Aldrich cat. # E9379) after it has been run on a 15% polyacrylamide denaturing gel using the ImageQuant RT ECL Imager from GE Healthcare Life Science. Absorbance of DNA and RNA strand was determined by an HP 8453 diode-array spectrophotometer (Agilent, Germany). And DNA and RNA concentrations were determined from their absorbance at λ = 260 nm with reference at 800 nm and extinction coefficients determined by Oligocalc.[106] Purified DNA was lyophilized before placing in the -20 °C freezer for future use.

Table 3. 1 DNA and RNA sequences for amplification.

RNA	**5'-UGU CAG UUG UUG UUC GAU UGA UUC CAU-3'**
nm RNA	5'- UGA GAC CCU AAC UUG UGA UGU UUA CCG-3'
mm RNA	5'-UGU CAG UUG UUG UUC GAU GGA UUC CAU-3'
cDNA	5'-ATG GAA TCA ATC GAA CAA-3'
DNA-IIa	5'-pATC GAA CAA-3'
DNA-IIb	5'-ATG GAA TCA-3'
F-DNA-IIb	5'-T_FATG GAA TCA-3'
F-DNA-Ia'	5'-T_FTG TTC GA-3'
F-DNA-Ia	5'-T_FTG TCC GA-3'
DNA-Ia	5'-TTG TCC GA-3'
DNA-Ib	5'-p(Ab) TGA TTC CAT-3'
dDNA	5'-TC GAA CAA CAA CTG ACA-3'
F-DNA-I'	5'-T_FTG TTC GAT (Ab) TGA TTC CAT-3'
DNA-I	5'-TTG TTC GAT TGA TCC CAT-3'
F-DNA-I	5'-T_FTG TTC GAT (Ab) TGA TCC CAT-3'

T_F: fluorescein-modified thymidine, p: phosphate, Ab: abasic lesion

Table 3. 2 DNA sequences for colorimetric detection with DNA-modified AuNPs

Probe A	**5'-SS-C6 -AAA AAA AAA AAT GG AAT CA-3'**
Probe B	5'-ATC GAA CAA AAA AAA AAA A-C3-SS-3'
(A_5)Linker(A_5)	5'-AAAAA TTG TTC GAT TGA TTC CAT AAAAA-3'
(T_5)cDNA(T_5)	5'-TTTTT ATG GAA TCA ATC GAA CAA TTTTT-3'
DNA-IIa(T_5)	5'-pATC GAA CAA TTTTT-3'
(T_5)DNA-IIb	5'-TTTTT ATG GAA TCA-3'

SS-C6: Thiol-Modifier C6 S-S (Cat # 10-1936)

C3-SS: 3'-Thiol-Modifier C3 S-S CPG (Cat# 20-2933)

3.2.2 Synthesis of Gold nanoparticles

13 nm diameter gold nanoparticles were synthesized following the method established by the Turkevich Synthesis.[107-108] In brief, all glassware used in the synthesis was soaked in aqua regia, following by washing at least three times with milliQ water and then dried in an oven at around 100 °C before use. Gold(III) chloride trihydrate (0.0985 g, 0.25 mmol-) was dissolved in MilliQ water (250 mL) and then placed in a round bottom flask with a stir bar and refluxed, by heating in an oil bath set to 120 °C. After 20 minutes, trisodium citrate solution (25 mL, 38.8 mM) was added to the refluxing solution. Once addition of the trisodium citrate solution, the colour of the mixture turned from light yellow, to black and to dark wine-red at the end. After refluxing for another 10 minutes, the mixture was cooled to room temperature and filtered through a polyethersulfone (PES) filter with 0.45 μm pores (Catalogue # 10040-462, VWR). The 13-nm gold nanoparticles were characterized by UV-vis absorbance spectroscopy based on their characteristic absorbance peak at λ = 519 nm. [109] The nanoparticle dispersion was stored in a plastic container in the dark at room temperature before use.

3.2.3 Preparation of DNA modified gold nanoparticles

DNA-modified gold nanoparticles were prepared according to the procedure of Lam et al.[103] with few modifications. Specifically, the thiolated DNA was generated by deprotecting the disulfide terminated strands, probe A and probe B, with a dithiothreitol (DTT) solution (0.1 M DTT, 0.18 M PBS, pH 8) for 2 hours. And then the thiolated DNA was purified by loading into a PD-10 desalting column (GE Healthcare, Catalogue # 17-0851-01) with PBS running buffer (50 mM PBS, 0.05 wt% SDS, 2.5 wt% NaN_3 pH = 7) and collected in fractions. UV-Vis absorbance at 260 nm was used to determine the amount of thiolated DNA in each fraction. For each batch of DNA-modified gold nanoparticles, the thiolated DNA probe strand (15 nmol) was immediately added to a citrate-capped 13-nm gold nanoparticle suspension (1 mL, ~1.5 x 10^{12} particles/mL), followed by water (3 mL) and topped up to 5 mL by buffer (50 mM PBS, 0.05 wt% SDS, 2.5 wt % NaN_3, pH = 7). Thereafter, this mixture was salted up to 0.05 M NaCl by addition of 2 M NaCl buffer (2 M NaCl, 10 mM PBS, 0.01 wt% SDS, 0.5wt % NaN_3, pH = 7). After sitting overnight, the mixture was further salted up to 0.3 M NaCl in 0.05 M NaCl increments using the 2 M NaCl buffer. Samples were also sonicated about 15 seconds and then sat 20 minutes in between salt additions. Generally, samples were incubated for at least two days before purification.

The purification process was created by Hurst et al.[110] The DNA-AuNP solution was transferred in several 2 mL tubes and topped up by 0.2 M NaCl buffer (10 mM PBS, 0.01 wt% SDS, 0.5 wt% NaN_3, pH = 7). After centrifuging at 14000 RPM for 30 minutes, each tube was decanted to remove free DNA and the remaining DNA-AuNP precipitate was resuspended in 0.2 M NaCl buffer (10 mM PBS, 0.01 wt% SDS, 0.5 wt% NaN_3, pH = 7). After repeating these steps three times, the concentration of DNA-AuNPs was determined by its molar absorptivity coefficient ε of 2.4 x 10^8 $M^{-1}cm^{-1}$ with UV-visible absorbance spectroscopy by monitoring at λ_{max} = 525 nm

with reference at 850 nm.[110-111] As demonstrated in Figure 3.2, the absorption peak of 13 nm AuNPs was 519 nm but it redshifted to 525 nm when gold nanoparticles modified by thiolated DNA. To make the aggregates, each DNA modified AuNP (1.5 pmol) and linker DNA (60 pmol) were combined and topped up to 100 µL with 0.2 M NaCl buffer (10 mM PBS, 0.01 wt% SDS, 0.5 wt% NaN_3, pH = 7). Newly mixture of DNA and AuNP were aliquoted to 10 uL each in 0.2 mL tubes and allowed to aggregate overnight.. Those aggregates was sonicated 15 seconds before use.

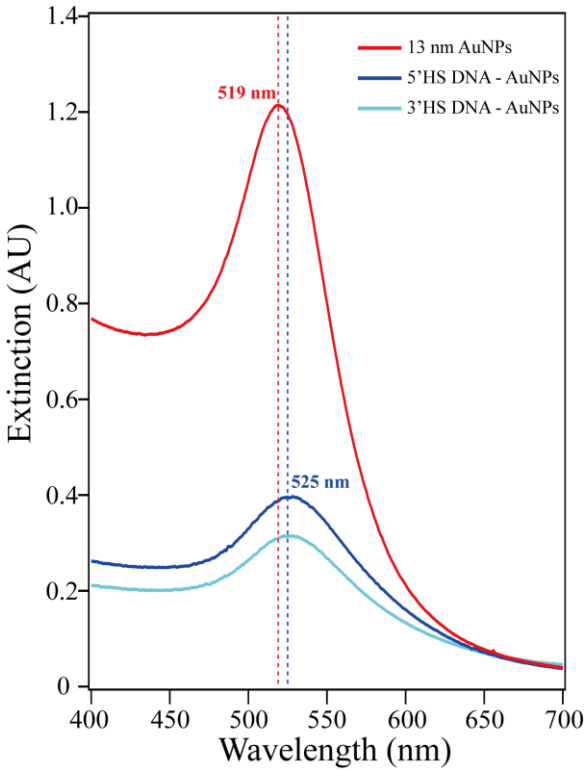

Figure 3. 2 Extinction of 13 nm gold nanoparticles and thiolated DNA modified gold nanoparticles.

3.3 Result and discussion

3.3.1 Lesion-induced DNA amplification for RNA

To achieve rapid isothermal RNA detection, the RNA was first transcribed into a complementary DNA (**cDNA**) using a RNA-templated DNA ligation. Then the **cDNA** is amplified in a cross catalytic cycles by using lesion-induced DNA amplification (LIDA).[71] Specifically, in step A, the target **RNA** hybridizes with two complementary DNA primers, **DNA-IIa** and **DNA-IIb**, to form an **RNA-DNA** nicked duplex, which is then ligated by T4 DNA ligase, the same enzyme used for DNA amplification (Figure 3.2). This **RNA-DNA** duplex then is denatured by a displacement DNA (**dDNA**), which is able to hybridize with the RNA target sequence and longer than **cDNA** due to an overhang region. Therefore, the **cDNA** is released because the **RNA-dDNA** duplex is more stable than the **RNA-cDNA** duplex. Once denatured, the **cDNA** sequence can hybridize to two complementary probes with destabilizing groups (Figure 3.2, cycle B). After templated ligation of these probes, the newly formed destabilizing template DNA (**F-DNA**) spontaneously dissociates from the product duplex because of the destabilizing groups. In the next step, **F-DNA** templates the ligation of two other probes, the same probes in step A, to form a copy of the **cDNA** (Figure 3.2, cycle C). This cross-catalytic replication of **cDNA** and **F-DNA** continues until all the probes are consumed. For colorimetric detection, we applied add overhangs onto DNA primers **DNA-IIa(T_5)** and **(T_5)DNA-IIb,** which were able to form **(T_5)**cDNA**(T_5)**.

It is important to note one current limitation of LIDA: even in the absence of initial RNA target a background process can trigger the formation of cDNA such that eventually cross-catalytic amplification of cDNA takes place.[70, 105] Therefore, the target initiated process has to be faster than this background-triggered process for the sample to test positive vs the negative control.

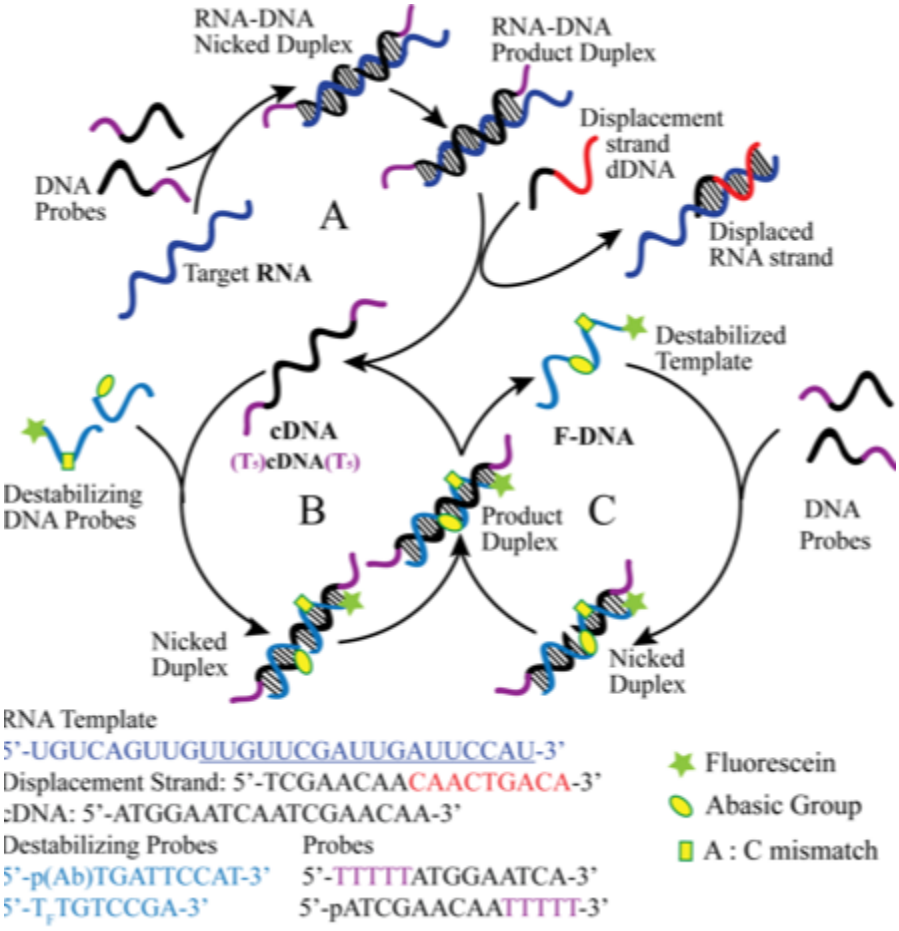

Figure 3. 3 Schematic illustrating reverse transcription lesion-induced DNA amplification (LIDA) by transcribing the RNA into a cDNA which is then amplified isothermally by LIDA. *Oval*: abasic lesion; *Square*: A: C mismatch; *Star*: fluorescent label.

3.3.2 Colorimetric detection of LIDA probes

The previous work by our group proved 10 pmol of DNA can be detected rapidly by the gold nanoparticle based platform using a different target sequence.[103] Based on this result, we prepared the aggregates using 150 fmol of each gold nanoparticle probe and 6 pmol **(A5)Linker(A5)** in 10 μL of the 0.2 M NaCl buffer for direct visualization experiments. Then different amounts of target

cDNA were added to aggregates respectively, keeping the total amount of volume at 20 μL (Figure 3.3 a). The pictures were taken after 10 minutes, showing that 10 pmol of the **(T_5)cDNA(T_5)** could be detected within 10 min (Figure 3.2 b). The LIDA steps involved four primers: namely **DNA-Ia, DNA-Ib, DNA-IIa(T_5)** and **(T_5)DNA-IIb**. A concern is that the primers may denature the gold nanoparticle aggregates. Therefore we aimed to discover if disaggregation could be triggered by the primers **DNA-IIa(T_5)** and **(T_5)DNA-IIb** used in LIDA (Figure 3.3 c), which would present a problem for our detection strategy. The addition of the same amount of the two LIDA primers showed that 10 pmol of each "half target" was also able to unfortunately displace the linker leading to disaggregation and a color change (Figure 3.3 d). However, the amplification mixture in LIDA contains four different primers (**DNA-Ia, DNA-Ib, DNA-IIa(T_5)** and **(T_5)DNA-IIb**), which are complementary and can form two double strands (Figure 3.3 e). We were pleased to see that combining all of these primers, 10 pmol of each, did not disturb the aggregates (Figure 3.3 f). Summarizing all of the results thus far, both 10 pmol of target (b2) and half-targets (d4) were capable of displacing the linker, but the four primer mixture did not, which we attribute to these primers being complementary to each other preventing them from triggering disaggregation. These experiments indicate our approach is promising for using AuNP disaggregation to detect DNA biomarkers amplified by LIDA.

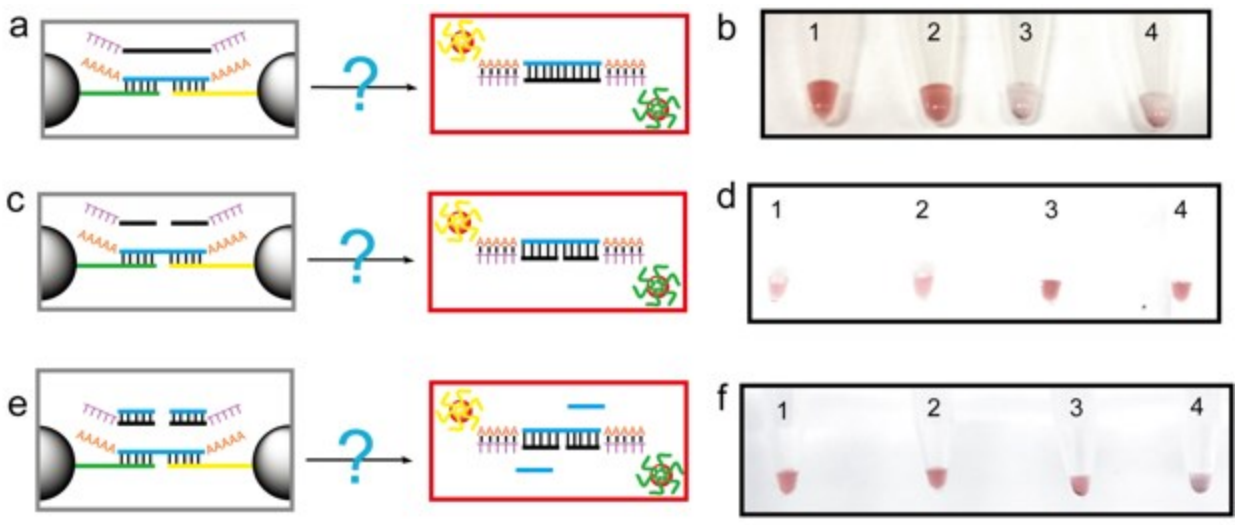

Figure 3. 4 Colorimetric experiments of primers of LIDA. (a) Scheme of denaturation of aggregates by target with overhangs **(T_5)cDNA(T_5)**. (b) Image of aggregate solution 10 minutes after adding the **(T_5)cDNA(T_5)** target to the pre-formed AuNP aggregates: 1) 100 pmol, 2) 10 pmol, 3) 1 pmol, 4) 0 pmol of the **(T_5)cDNA(T_5)** target added. (c) Scheme of denaturation of aggregates by half-targets (primers) **DNA-IIa(T_5)** and **(T_5)DNA-IIb**. (d) Image of aggregate solution 10 minutes after adding: 1) 40 pmol, 2) 30 pmol, 3) 20 pmol, 4) 10 pmol of each primer **DNA-IIa(T_5)** and **(T_5)DNA-IIb**. (e) Scheme of denaturation of aggregates by the four primers **DNA-Ia, DNA-Ib, DNA-IIa(T_5)** and **(T_5)DNA-IIb**. (f) Image of aggregate solution 10 minutes after adding: 1) 70 pmol, 2) 50 pmol, 3) 30 pmol, 4) 10 pmol of each **DNA-Ia, DNA-Ib, DNA-IIa(T_5)** and **(T_5)DNA-IIb**.

3.3.3 Colorimetric detection of DNA cross-catalytic amplification

Prior to determining our main objective of coupling our colorimetry method with the detection of RNA, we wanted to see if our AuNP based disaggregation method was compatible with LIDA amplification of a DNA target. Therefore first the following procedure was used. Single-stranded **cDNA** (203 fmol), primer **DNA-Ia** (20.3 pmol), primer **DNA-Ib (**40.6 pmol), primer **DNA-IIb (**40.6 pmol) and primer **DNA-IIa (**40.6 pmol) were combined in a 600 µL microtube. The reaction was topped up to 10 µL by MQ water and was incubated at 28 °C. A similar experiment but without

cDNA as a control was prepared at the same time. To these mixtures, 5 μL of master mix (comprising 1 μL T4 DNA ligase, 20000 cohesive end unit, 2.5 μL water and 1.5 μL T4 DNA ligase buffer from New England Biolabs) were added and a timer was started. The amount of **(T_5)cDNA(T_5) would increase due to the ligation between DNA-Ia and DNA-Ib, DNA-IIb.**

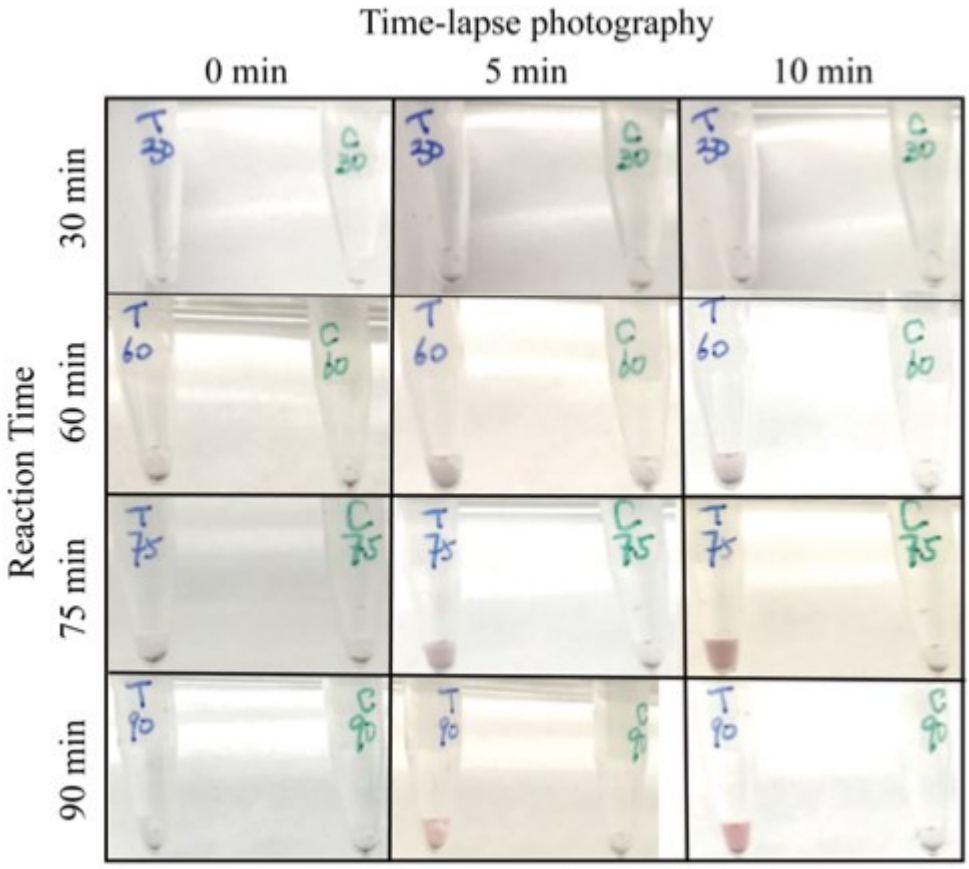

Figure 3. 5 The results of colorimetric detection of DNA cross-catalytic amplification at 28 °C. The pictures of the addition of the amplification reaction at 30, 60, 75 and 90 minutes were shot 0, 5 and 10 minutes after solution transfer. *Blue* with cDNA, *Green* without cDNA.

We noticed that the aggregates exhibited a tiny bit of pink colour after addition of just water, (Figure 3.4b4). To minimize this unwanted colour change, the aggregates were lyophilized in advance and then rehydrated in 10 μL of water before use. We noticed that the aggregates appeared

more stable that the disaggregation took longer time after lypholization. Next, 3 μL of the LIDA reaction solution was added to the rehydrated aggregates at different time points, and a picture was taken after 0, 5 and 10 minutes. If the yield of the amplification was 100%, the 3 μL solution would contain around 4 pmol of **(T_5)cDNA(T_5)**. As shown in Figure 3.4, a clear pink colour appeared in 5 minutes after addition of solution from the 90-minute reaction in the presence of 1 mol% initial **cDNA** template while the control experiment (with 0 mol% initial template) still kept the black aggregates at the bottom of the eppendorf tube. Additionally, the difference in colour of the aggregate solution with and without target was found to be even more significant 10 minutes after addition. This experiment proved the LIDA amplification method was compatible with the gold nanoparticle based colorimetric detection and allowed us to increase the sensitivity of detecting cDNA from 10 pmol to at least ~200 fmol.

3.3.4 Colorimetric detection of RNA transcription with lesion induced DNA amplification

The scheme of RNA transcription with lesion induced DNA amplification was shown in Figure 3.1. Single-stranded **RNA** (102 fmol) for the templated reaction or no initial RNA for the control were combined with primers **DNA-IIb (**40.6 pmol) and **DNA-IIa (**40.6 pmol) in a 0.6 mL eppendorf tube. The reactions were topped up to 5 μL using nuclease free water (NFW) and incubated at 28 °C. To these mixtures, 1 μL T4 DNA ligase, 20000 cohesive end unit, and 3 μL buffer (500 mM Tris-HCL, 100 mM $MgCl_2$ and 10 mM ATP, pH = 7.5) were added together, and a timer was started. The reactions were allowed to react at 28 °C for 15 minutes. While waiting, master mix was prepared, which contained **DNA-Ib (**40.6 pmol), **dDNA (**40.6 pmol), **DNA-Ia (**20.3 pmol), ATP (3 μL**,** 100 mM) and T4 DNA ligase buffer (3 μL, from New England Biolabs). Finally master mix was topped up with water to 7.5 μL. Then 7.5 μL of master mix was pipetted

into the reaction tube after the 15 minute time lapse. Then the reaction tube was kept in the incubator at 28 °C, and the timer was restarted again.

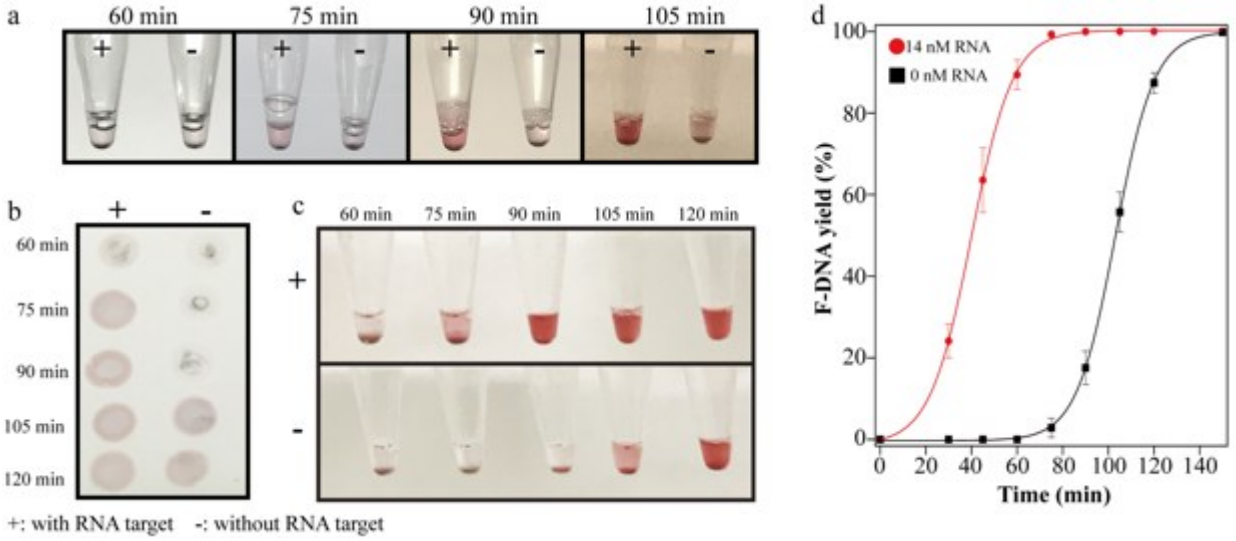

Figure 3. 6 (a) Picture of aggregated DNA modified AuNPs 15 minutes after the addition of 3 µL aliquot from tube + (102 fmol, RNA target) and - (no target control) from 15 µL standard RNA-templated LIDA reactions allowed to commence the specified time. (b) 5 µL of solution from each tube + and - shown in (c) was dropped onto a TLC plate. (c) Experiment shown in (a) of DNA-gold nanoparticle aggregates 15 minutes after the addition of amplification aliquot to the last tube. At this time, the 90-minute sample had been sitting for 45 minutes since the amplification aliquot was added, which allowed the colour to develop more fully for the RNA positive sample. (d) Gel electrophoresis results of formation of **F-DNA** initiated by 102 fmol and 0 mol RNA with time.

After amplification, 3 µL of the reaction solution was added to the rehydrated AuNP aggregates at different time points. The pictures were taken 15 minute after each addition of the amplification solution. After 75 minutes of amplification, the addition of the reaction aliquot led to disaggregation and rapid colour change from black/purple to red in 15 minutes when RNA was present (Figure 3.6 a). On the other hand, no colour change was observed until the LIDA step had proceeded 105 minutes when RNA template was absent. To visualize this colour comparison by

another method, 5 μL of these aggregate mixtures after the amplification reaction had been added were pipetted onto a silica coated TLC plate (Figure 3.6 b). The picture of all T tubes (with RNA) and C tubes (without RNA) was taken after 15 minutes of the addition of the amplification mixtures to the last tube (Figure 3.6 c). As shown in Figure 3.6 d, the gel electrophoresis results also proved the significant different amplification yield at 75 minutes and 90 minutes as same as colorimetric detection.

3.3.5 Selectivity of gold nanoparticle-based colorimetric detection

Next, the selectivity of the assay was investigated by comparing RNA-triggered LIDA using three different RNA including the complementary target RNA (matched RNA), a one-base mismatched RNA (**mmRNA**) and a completely non-matched RNA strand (**nmRNA**). The concentration of **F-DNA**, complementary to **cDNA**, was evaluated at 60 min (red bar), 75 min (blue bar) and 90 min (green bar) for amplification reactions initiated by 140 nM of these different RNA sequences using polyacrylamide gel electrophoresis (Figure 3.7). As expected, based on our previous work that showed excellent selectivity of LIDA for single base mismatched, [112] there was a significant difference in **F-DNA** formed between the **matched RNA** strand compared to the **mmRNA** and **nmRNA** target. Moreover, the gel results were matched by colorimetric detection as seen in Figure 3.6b where the first colour change was observed when the LIDA step had proceeded 75 minutes but only for the **matched RNA**. Interestingly, the gold nanoparticle aggregates remained black precipitates even after 120-minute of **nm RNA** when the no-target control experiment had changed to pink colour (Figure 3.6c), which was expected as same as the no RNA result.

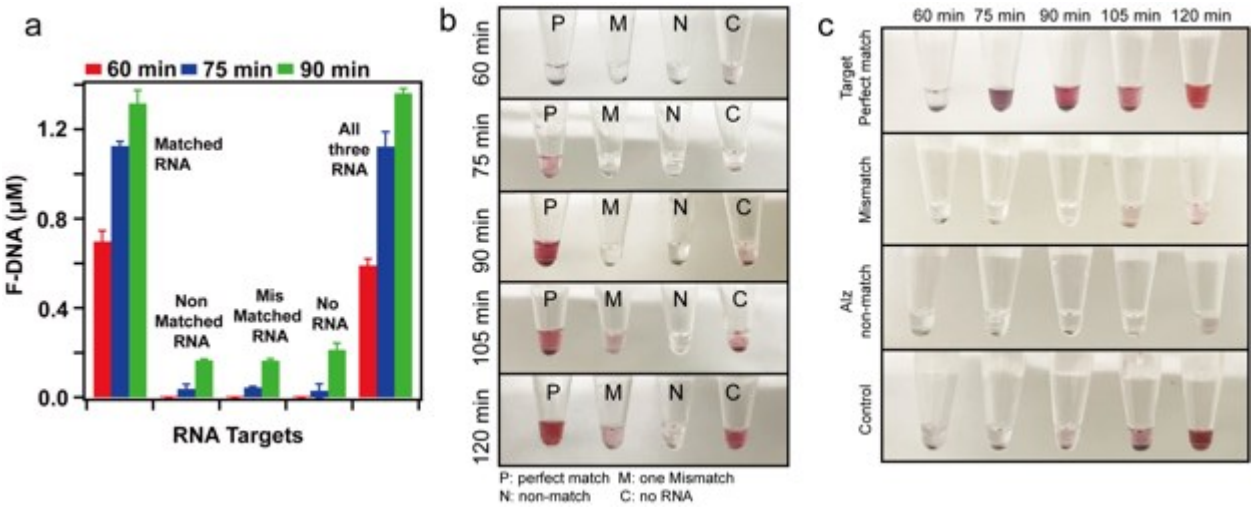

Figure 3. 7 Specificity of colorimetric detection with reverse transcription LIDA. (a) Formation of **F-DNA** initiated by various targets: matched RNA, non-matched RNA, one base mismatched RNA, no RNA and all RNA together. Red, blue and green represent 60 min, 75 min and 90 min time point of the reaction. (b) Picture of aggregated DNA modified AuNPs 15 minutes after the addition of 3 μL aliquot from various targets: matched RNA, non-matched RNA, one base mismatched RNA, no RNA ('Control'). (c) All the tubes of DNA-gold nanoparticle aggregates shown in (b), 15 minutes after the addition of the 120-minute LIDA amplification aliquot.

To further confirm the selectivity in real biological samples, 102 fmol of matched target RNA was spiked into 4 μg human lungs total RNA (**HLTR**) samples (1 μg/μL) extracted from cells. As seen in Figure 3.7a, the gel electrophoresis reaction showed the formation of **F-DNA** for the templated (red) reaction was faster than the non-templated (black) reaction even though total RNA was present. Similarly, a clear pink colour appeared in 15 minutes after addition of solution from 90-minute reaction with the **matched RNA** template in **HLTR (**Figure 3.7b**)**. Also, after 90-minute reaction, there were still differences between with and without target in **HLTR**. The picture was taken 15 minutes after all the LIDA step proceeded. The colour of this experiment changed

from pink to dark wine red over time and several tubes were turning to greyish colour (Figure 3.7c). The possible reason would be other strands in human lungs total RNA makes the DNA-gold nanoparticles aggregate again.

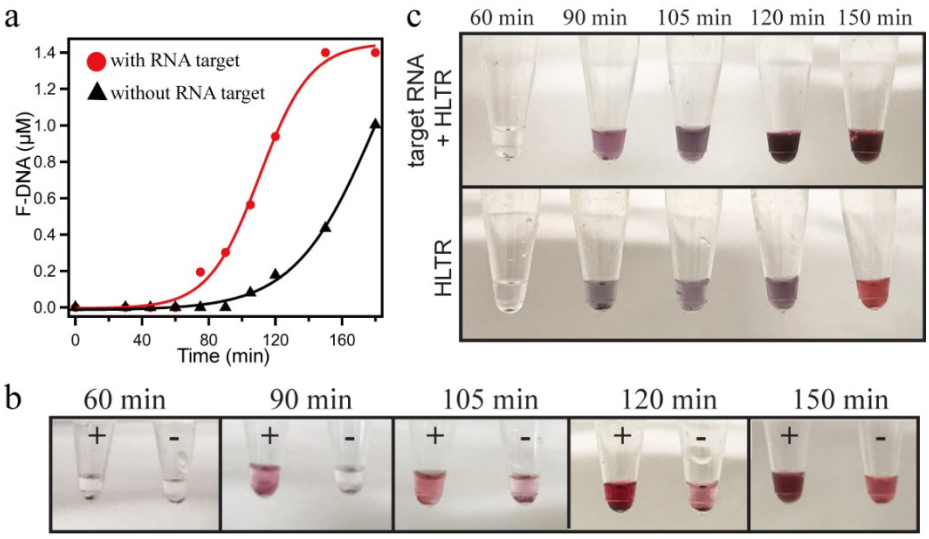

Figure 3. 8 Specificity of colorimetric detection with reverse transcription LIDA in human lungs total RNA. (a) Formation of **F-DNA** initiated by 102 fmol and 0 mol RNA with time. b) Picture of aggregated DNA modified AuNPs 15 minutes after the addition of 3 μL aliquot from tube T (RNA target) and C (no target control). (c) All tubes DNA-gold nanoparticle aggregates 15 minutes after the addition from LIDA reaction to the last tube.

3.3.6 Reduction of DNA modified gold nanoparticle aggregates

To improve sensitivity, our hypothesis was that aggregates made from less AuNP and linker would require less **(T_5)cDNA(T_5)** to trigger the disassembly. Therefore we prepared aggregates using 50% of the amount used in the previous aggregates, specifically 75 fmol of each gold nanoparticle probe and 3 pmol of **(A_5)Linker(A_5)** were combined in the 0.2 M NaCl buffer overnight, followed by lyophilization. Then different amounts of targets were added to aggregates

respectively, keeping the total amount of volume at 20 μL (Figure 3.8 a). The picture were taken after 10 minutes, showing 4 pmol (0.2 μM) of the **(T_5)cDNA(T_5)** could be detected. We also made aggregates consisting of 33.3% of the original aggregate amounts 50 fmol gold nanoparticle probes and 2 pmol **(A_5)Linker(A_5)** in the 0.2 M NaCl buffer. As shown in Figure 3.8b these less concentrated aggregated showed faint but discernable colour difference between the addition of 2 pmol (0.29 μM) and 3 pmol (0.43 μM) **(T_5)cDNA(T_5)** into 33.3% aggregates, keeping the total volume is 7 μL.

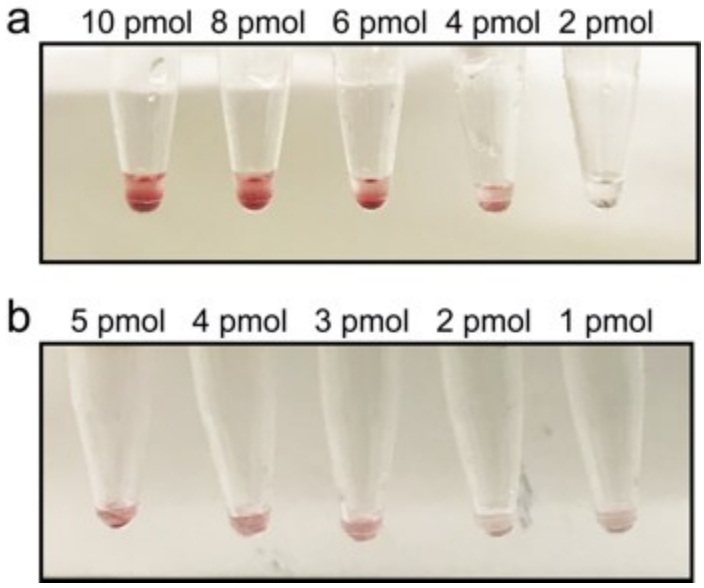

Figure 3. 9 Colorimetric experiments of **(T_5)cDNA(T_5)** target with lower amount of aggregates. (a) 50% aggregates of original work. 4 pmol (0.2 μM) of **(T_5)cDNA(T_5)** disassembled aggregates in 20 μL solution. (b) 33.3% aggregates of original work. 3 pmol (0.43 μM) of **(T_5)cDNA(T_5)** disassembled aggregates in 7 μL solution. Pictures were taken 10 minutes after addition of **(T_5)cDNA(T_5)**.

3.3.7 Colorimetric detection with less aggregates after RNA amplification

Based on the previous work, we reduced **RNA** to different amounts, namely 10.2 fmol, 1.02 fmol, 102 amol, spiked into human lungs total RNA (**HLTR**) samples (5 µg/15 µL). Also, half of primers **dDNA (**20.3 pmol), **DNA-IIb (**20.3 pmol). and **DNA-IIa (**20.3 pmol), **DNA-Ib (**20.3 pmol), **DNA-Ia (**10.2 pmol) were used in LIDA but other conditions remained. 7.5 µL of the amplification solution was added into lyophilized 33.3% aggregates at different time points (Figure 3.9a). Both gel electrophoresis and colorimetric detection showed the difference between with and without target after 2.25-hour amplification. As seen in Figure 3.9c, all additions of 10.2 fmol, 1.02 fmol and 102 amol RNA after amplification disassembled gold nanoparticle aggregates successfully. However, the faint pink colour appeared after addition of 2.5-hour LIDA without RNA target.

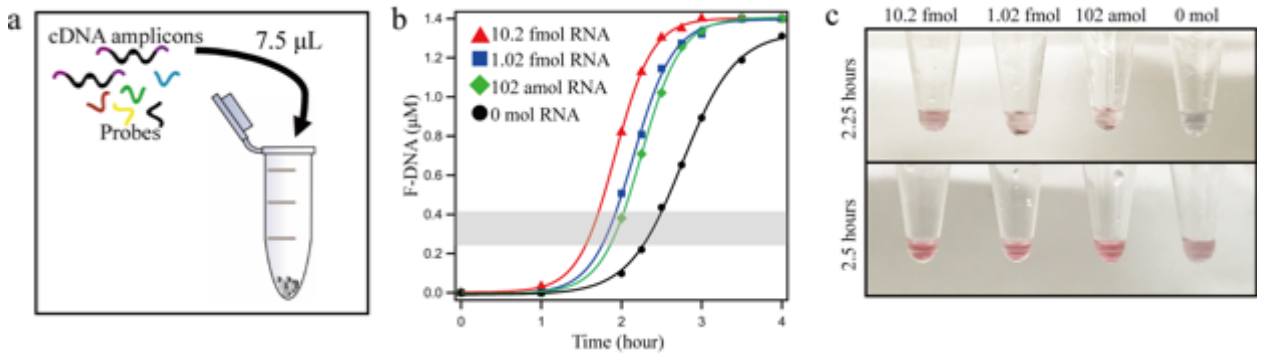

Figure 3. 10 Reverse transcription LIDA with gel electrophoresis and colorimetric detection. (a) Schematic illustrating the addition of amplicons and probes into lyophilized aggregates. (b) Formation of **F-DNA** initiated by 10.2 fmol, 1.02 fmol, 102 amol, and 0 mol RNA in human lungs total RNA with time. (c) Picture of reduced aggregated DNA modified AuNPs (33.3% of the original amount described in Chapter 3.3.6) 15 minutes after the addition of 7.5 µL aliquot from various targets.

Regarding the experimental results, the DNA-gold nanoparticle aggregates were able to detect 102 amol of RNA target in human lungs total RNA. However, this strategy has a limitation that the speeds of amplifications of RNA target and no RNA target (Figure3.10) have a different colour change but not as significant as high concentration experiments (Figure 3.8). The successful detection may require the specific amplification time, for example, the low concentration RNA target in human lungs total RNA need to specifically amplify around 2.25 hours. It means it need to operate at special time, which is not convenient. Therefore, controlling the amplification steps is an idea to optimize this method in the future. Also, the colour of disassembled gold nanoparticle is faint compared with control experiments, so this is another direction to improve this method.

3.4 Conclusion

In this study we have developed a system based on the target-triggered disassembly of DNA-gold nanoparticle aggregates that is rapidly and able to expand LIDA to the detection of RNA biomarkers. Although the presence of two LIDA primers triggered disassembly, we serendipitously found that the presence of all four primers did not trigger aggregate dissolution. Therefore amplification by LIDA could be directly combined with our colorimetric detection method allowing us to detect within 10 minutes after 90-minute amplification at 28 °C. Also, we combined RNA transcription with LIDA and DNA-gold nanoparticles at room temperature to achieve this rapid detection after 90-minute amplification. To discover the selectivity of this detection, we tested single-base mismatch RNA, non-match RNA, and target RNA in human lungs RNA. The colorimetric method showed good selectivity from those impurities. Afterwards, we used less aggregates to improve the limits of detection and achieve the detection of 102 amol RNA. The major limits of this colorimetric system are that the most sensitive assay requires long

amplification times (2.25 hours) and leads to only faint color changes. As such, these limits should be addressed in the future work.

Chapter 4

Concluding Remarks and Future Work

4.1 General conclusion

This thesis has described applications of assembly and disassembly of colloids. These systems have been explored over decades. The goal of this work is to fill the gaps of previous researches.

Researchers have built chemical reaction network about dissipative self-assemblies, including nanoparticles,[61] fibres,[60, 68] supramolecular polymers,[69] and active droplets[67]. To enhance this network, in Chapter 2, we reported a dissipative self-assembly of amphipathic molecules into spherical micelles triggered by a chemical fuel. The amphipathic molecules were synthesized by CuAAC reaction to combine a hydrophilic chain and a dissipative hydrophobic molecules. Then we preformed this molecule to kinetic experiments by HPLC to determine the half-life. Upon that, using fluorescence spectroscopy to check the emission maximum of Nile red confirmed the self-assembly of amphipathic molecule by a blue shift from 651 nm to 618 nm after addition of fuel. Then we continued to confirm the assembly by DLS experiments that showed the assembly and dissipation of micelles. Finally, we used Cryo-EM to image the assembled micelles where we found that the size of micelles was around 3 nm after 3 minutes of EDC addition. Based on those results, we demonstrated that we are able to build a new strategy to form amphipathic molecules and regulate the lifetime of these assemblies by adjusting the initial fuel.

Also, disassembly of colloid plays a significant role in biomarker detection. One of the well-known techniques is colorimetric detection based on DNA disassembly proc ess using DNA-gold nanoparticles. Here, we reported on a colorimetric detection method for RNA detection using the rapid disassembly of DNA-gold nanoparticle aggregates at room temperature in Chapter 3. We applied all four primers of lesion induced DNA amplification (LIDA)[70-71] to DNA-gold nanoparticles aggregates,[46] finding that primers would not trigger the disassembly process. Before adapting to RNA template, we found that 203 fmol target DNA was able to trigger the DNA-gold

nanoparticle within 10 minutes after 90-minute LIDA amplification at room temperature. Upon that, we combined RNA transcription with LIDA and DNA-gold nanoparticles at 28 °C to achieve room temperature colorimetric detection as low as 102 fmol target RNA. Also, we performed a selectivity experiments between three targets, matched RNA, mismatched RNA and non matched RNA and showed a significant difference in colorimetric detections between the various targets. Additionally, we reduced the aggregates to achieve 102 amol target RNA in human lungs total RNA after amplification.

4.2 Future Plans

4.2.1 Chemical reaction network of dissipative self-assembly of amphipathic molecules into spherical micelles.

We have showed one example of dissipative self-assembly micelles using on amphipathis molecule. We want to expand our library by synthesizing more amphipathic molecules. Therefore, we plan to synthesize a new molecule called 4-(1-((3R,4S,5R,6R)-3,4,5-trihydroxy-6-(hydroxymethyl)tetrahydro-2H-pyran-2-yl)-1H-1,2,3-triazol-4-yl)phthalic acid shown in Figure 4.1a. To further prove the fuel-driven method can be used to assembly of micelles, we will use the same analytical method as Chapter 2 to determine the process.

Additionally, we plan on discussing of the differences between dissipative self-assembly and normal self-assembly micelles. Di(ethylene glycol) benzyl ether (Figure 4.1b) is one of the choices due to its commercial available and the similar structure.

Our German partners will continually work on those two points to optimize the chemical reaction network

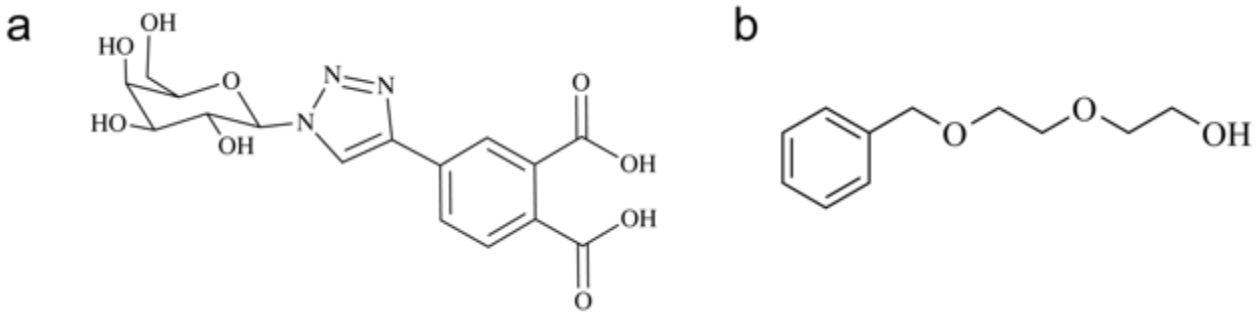

Figure 4. 1 The scheme of molecules (a) different 4-(1-((3R,4S,5R,6R)-3,4,5-trihydroxy-6-(hydroxymethyl) tetrahydro-2H-pyran-2-yl)-1H-1,2,3-triazol-4-yl)phthalic acid. (b) Di(ethylene glycol) benzyl ether.

4.2.2 Optimization of the colorimetric detection based on DNA-gold nanoparticle aggregates.

We used two separated steps to achieved the colorimetric detection but those steps may not fit the requirements of point-of-care (POC) detection due to the relatively difficult operation.[113-114] Herein, we are trying to design and build an all-in-one equipment to deal with this problem.

First of all, we used an amplification method that all primers and enzyme were dissolved in liquid in advance. It is a multiple step that to pipette multiple solutions into an eppendrof. I think building an amplification method operated with lyophilized primers and enzyme would be able to deal with this problem.

Then, we hope that we could handle the two-steps in one appliance.An idea of designing a three-layer equipment is shown in Figure 4.2. The first layer contains lyophilized primers and enzyme and then fill with suitable volume of sample. The bottom of the first is a switcher that it

turned off when the sample is amplifying. Turning on the switcher lets the solution flow into the second layer.

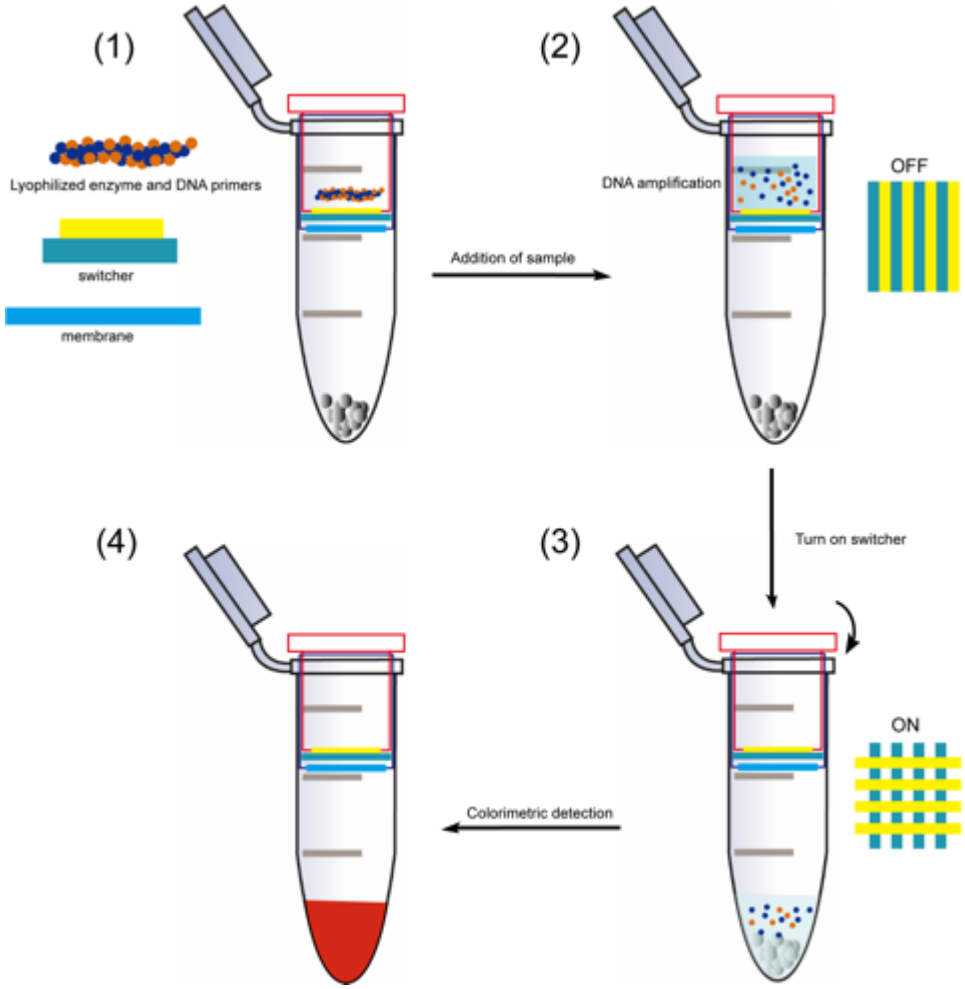

Figure 4. 2 Schematic all-in-one equipment of DNA/RNA amplification and colorimetric detection.

Our final goal is to detect from real sample such as saliva that contains larger molecules like enzymes.[115] Hence, a membrane between the second and third layers to filter the large molecules would be able to reduce the influence of other molecules that can interfere with the results.

Reference

1. Philp, D.; Stoddart, J. F., Self-assembly in natural and unnatural systems. *Angew Chem Int Edit* **1996,** *35* (11), 1154-1196.

2. Lis, L. J.; Mcalister, M.; Fuller, N.; Rand, R. P.; Parsegian, V. A., Interactions between Neutral Phospholipid-Bilayer Membranes. *Biophys J* **1982,** *37* (3), 657-665.

3. Whitesides, G. M.; Grzybowski, B., Self-assembly at all scales. *Science* **2002,** *295* (5564), 2418-2421.

4. Caplan, M. R.; Moore, P. N.; Zhang, S. G.; Kamm, R. D.; Lauffenburger, D. A., Self-assembly of a beta-sheet protein governed by relief of electrostatic repulsion relative to van der Waals attraction. *Biomacromolecules* **2000,** *1* (4), 627-631.

5. Aakeroy, C. B.; Beatty, A. M.; Helfrich, B. A., "Total synthesis" supramolecular style: Design and hydrogen-bond-directed assembly of ternary supermolecules. *Angew Chem Int Edit* **2001,** *40* (17), 3240-3242.

6. Lin, N.; Stepanow, S.; Vidal, F.; Kern, K.; Alam, M. S.; Stromsdorfer, S.; Dremov, V.; Muller, P.; Landa, A.; Ruben, M., Surface-assisted coordination chemistry and self-assembly. *Dalton T* **2006,** (23), 2794-2800.

7. Chen, Z. J.; Stepanenko, V.; Dehm, V.; Prins, P.; Siebbeles, L. D. A.; Seibt, J.; Marquetand, P.; Engel, V.; Wurthner, F., Photoluminescence and conductivity of self-assembled pi-pi stacks of perylene bisimide dyes. *Chem-Eur J* **2007,** *13* (2), 436-449.

8. Ghosh, S. K.; Nath, S.; Kundu, S.; Esumi, K.; Pal, T., Solvent and ligand effects on the localized surface plasmon resonance (LSPR) of gold colloids. *J Phys Chem B* **2004,** *108* (37), 13963-13971.

9. Qiu, P. H.; Jensen, C.; Charity, N.; Towner, R.; Mao, C. B., Oil Phase Evaporation-Induced Self-Assembly of Hydrophobic Nanoparticles into Spherical Clusters with Controlled Surface Chemistry in an Oil-in-Water Dispersion and Comparison of Behaviors of Individual and Clustered Iron Oxide Nanoparticles. *J Am Chem Soc* **2010,** *132* (50), 17724-17732.

10. Calero, C.; Faraudo, J.; Bastos-Gonzalez, D., Interaction of Monovalent Ions with Hydrophobic and Hydrophilic Colloids: Charge Inversion and Ionic Specificity. *J Am Chem Soc* **2011,** *133* (38), 15025-15035.

11. Conrad, M. J.; Singer, S. J., The Solubility of Amphipathic Molecules in Biological-Membranes and Lipid Bilayers and Its Implications for Membrane-Structure. *Biochemistry-Us* **1981,** *20* (4), 808-818.

12. Dominguez, A.; Fernandez, A.; Gonzalez, N.; Iglesias, E.; Montenegro, L., Determination of critical micelle concentration of some surfactants by three techniques. *J Chem Educ* **1997,** *74* (10), 1227-1231.

13. Yoshii, N.; Okazaki, S., A molecular dynamics study of structural stability of spherical SDS micelle as a function of its size. *Chem Phys Lett* **2006,** *425* (1-3), 58-61.

14. Yang, J., Viscoelastic wormlike micelles and their applications. *Curr Opin Colloid In* **2002,** *7* (5-6), 276-281.

15. Braun, P. V.; Stupp, S. I., CdS mineralization of hexagonal, lamellar, and cubic lyotropic liquid crystals. *Mater Res Bull* **1999,** *34* (3), 463-469.

16. Boekhoven, J.; van Rijn, P.; Brizard, A. M.; Stuart, M. C. A.; van Esch, J. H., Size control and compartmentalization in self-assembled nano-structures of a multisegment amphiphile. *Chem Commun* **2010,** *46* (20), 3490-3492.

17. Cushing, B. L.; Kolesnichenko, V. L.; O'Connor, C. J., Recent advances in the liquid-phase syntheses of inorganic nanoparticles. *Chem Rev* **2004,** *104* (9), 3893-3946.

18. Turkevich, J.; Stevenson, P. C.; Hillier, J., A Study of the Nucleation and Growth Processes in the Synthesis of Colloidal Gold. *Discuss Faraday Soc* **1951,** (11), 55-75.

19. Nehl, C. L.; Liao, H. W.; Hafner, J. H., Optical properties of star-shaped gold nanoparticles. *Nano Lett* **2006,** *6* (4), 683-688.

20. Chen, J. Y.; Wiley, B.; Li, Z. Y.; Campbell, D.; Saeki, F.; Cang, H.; Au, L.; Lee, J.; Li, X. D.; Xia, Y. N., Gold nanocages: Engineering their structure for biomedical applications. *Adv Mater* **2005,** *17* (18), 2255-2261.

21. Gole, A.; Murphy, C. J., Seed-mediated synthesis of gold nanorods: Role of the size and nature of the seed. *Chem Mater* **2004,** *16* (19), 3633-3640.

22. Jain, P. K.; Lee, K. S.; El-Sayed, I. H.; El-Sayed, M. A., Calculated absorption and scattering properties of gold nanoparticles of different size, shape, and composition: applications in biological imaging and biomedicine. *J Phys Chem B* **2006,** *110* (14), 7238-7248.

23. Su, K. H.; Wei, Q. H.; Zhang, X.; Mock, J. J.; Smith, D. R.; Schultz, S., Interparticle coupling effects on plasmon resonances of nanogold particles. *Nano Lett* **2003,** *3* (8), 1087-1090.

24. Sanchez-Iglesias, A.; Grzelczak, M.; Altantzis, T.; Goris, B.; Perez-Juste, J.; Bals, S.; Van Tendeloo, G.; Donaldson, S. H.; Chmelka, B. F.; Israelachvili, J. N.; Liz-Marzan, L. M., Hydrophobic Interactions Modulate Self-Assembly of Nanoparticles. *Acs Nano* **2012,** *6* (12), 11059-11065.

25. Feke, D. L.; Prabhu, N. D.; Mann, J. A.; Mann, J. A., A Formulation of the Short-Range Repulsion between Spherical Colloidal Particles. *J Phys Chem-Us* **1984,** *88* (23), 5735-5739.

26. Donaldson, S. H.; Lee, C. T.; Chmelka, B. F.; Israelachvili, J. N., General hydrophobic interaction potential for surfactant/lipid bilayers from direct force measurements between light-modulated bilayers. *P Natl Acad Sci USA* **2011,** *108* (38), 15699-15704.

27. Wilner, O. I.; Willner, I., Functionalized DNA Nanostructures. *Chem Rev* **2012,** *112* (4), 2528-2556.

28. McLaughlin, C. K.; Hamblin, G. D.; Sleiman, H. F., Supramolecular DNA assembly. *Chem Soc Rev* **2011,** *40* (12), 5647-5656.

29. Rothemund, P. W. K., Folding DNA to create nanoscale shapes and patterns. *Nature* **2006,** *440* (7082), 297-302.

30. Andersen, E. S.; Dong, M.; Nielsen, M. M.; Jahn, K.; Subramani, R.; Mamdouh, W.; Golas, M. M.; Sander, B.; Stark, H.; Oliveira, C. L. P.; Pedersen, J. S.; Birkedal, V.; Besenbacher, F.; Gothelf, K. V.; Kjems, J., Self-assembly of a nanoscale DNA box with a controllable lid. *Nature* **2009,** *459* (7243), 73-75.

31. Bujold, K. E.; Lacroix, A.; Sleiman, H. F., DNA Nanostructures at the Interface with Biology. *Chem-Us* **2018,** *4* (3), 495-521.

32. Seeman, N. C.; Sleiman, H. F., DNA nanotechnology. *Nat Rev Mater* **2018,** *3* (1).

33. Cutler, J. I.; Auyeung, E.; Mirkin, C. A., Spherical nucleic acids. *J Am Chem Soc* **2012,** *134* (3), 1376-1391.

34. Jin, R. C.; Wu, G. S.; Li, Z.; Mirkin, C. A.; Schatz, G. C., What controls the melting properties of DNA-linked gold nanoparticle assemblies? *J Am Chem Soc* **2003,** *125* (6), 1643-1654.

35. Nykypanchuk, D.; Maye, M. M.; van der Lelie, D.; Gang, O., DNA-guided crystallization of colloidal nanoparticles. *Nature* **2008,** *451* (7178), 549-552.

36. Saha, K.; Agasti, S. S.; Kim, C.; Li, X. N.; Rotello, V. M., Gold Nanoparticles in Chemical and Biological Sensing. *Chem Rev* **2012,** *112* (5), 2739-2779.

37. Xue, X.; Wang, F.; Liu, X., One-step, room temperature, colorimetric detection of mercury (Hg2+) using DNA/nanoparticle conjugates. *J Am Chem Soc* **2008,** *130* (11), 3244-3245.

38. Yurke, B.; Turberfield, A. J.; Mills, A. P.; Simmel, F. C.; Neumann, J. L., A DNA-fuelled molecular machine made of DNA. *Nature* **2000,** *406* (6796), 605-608.

39. You, M. X.; Chen, Y.; Zhang, X. B.; Liu, H. P.; Wang, R. W.; Wang, K. L.; Williams, K. R.; Tan, W. H., An Autonomous and Controllable Light-Driven DNA Walking Device. *Angew Chem Int Edit* **2012,** *51* (10), 2457-2460.

40. Tian, Y.; Mao, C. D., Molecular gears: A pair of DNA circles continuously rolls against each other. *J Am Chem Soc* **2004,** *126* (37), 11410-11411.

41. Dulkeith, E.; Morteani, A. C.; Niedereichholz, T.; Klar, T. A.; Feldmann, J.; Levi, S. A.; van Veggel, F. C. J. M.; Reinhoudt, D. N.; Moller, M.; Gittins, D. I., Fluorescence quenching of dye molecules near gold nanoparticles: Radiative and nonradiative effects. *Phys Rev Lett* **2002,** *89* (20), 203002.

42. Kang, K. A.; Wang, J.; Jasinski, J. B.; Achilefu, S., Fluorescence manipulation by gold nanoparticles: from complete quenching to extensive enhancement. *J Nanobiotechnology* **2011,** *9*, 16.

43. Dubertret, B.; Calame, M.; Libchaber, A. J., Single-mismatch detection using gold-quenched fluorescent oligonucleotides. *Nat Biotechnol* **2001,** *19* (4), 365-370.

44. Zhang, J.; Wang, L. H.; Zhang, H.; Boey, F.; Song, S. P.; Fan, C. H., Aptamer-Based Multicolor Fluorescent Gold Nanoprobes for Multiplex Detection in Homogeneous Solution. *Small* **2010,** *6* (2), 201-204.

45. Elghanian, R.; Storhoff, J. J.; Mucic, R. C.; Letsinger, R. L.; Mirkin, C. A., Selective colorimetric detection of polynucleotides based on the distance-dependent optical properties of gold nanoparticles. *Science* **1997,** *277* (5329), 1078-1081.

46. Xiao, R. P.; Wang, D. F.; Lin, Z. Y.; Qiu, B.; Liu, M. H.; Guo, L. H.; Chen, G. N., Disassembly of gold nanoparticle dimers for colorimetric detection of ochratoxin A. *Anal Methods-Uk* **2015,** *7* (3), 842-845.

47. Lam, M. K.; Gadzikwa, T.; Nguyen, T.; Kausar, A.; Alladin-Mustan, B. S.; Sikder, M. D.; Gibbs-Davis, J. M., Tuning Toehold Length and Temperature to Achieve Rapid, Colorimetric Detection of DNA from the Disassembly of DNA-Gold Nanoparticle Aggregates. *Langmuir* **2016,** *32* (6), 1585-90.

48. Al-Anati, L.; Petzinger, E., Immunotoxic activity of ochratoxin A. *J Vet Pharmacol Ther* **2006,** *29* (2), 79-90.

49. Schochetman, G.; Ou, C. Y.; Jones, W. K., Polymerase Chain-Reaction. *J Infect Dis* **1988,** *158* (6), 1154-1157.

50. Yan, L.; Zhou, J.; Zheng, Y.; Gamson, A. S.; Roembke, B. T.; Nakayama, S.; Sintim, H. O., Isothermal amplified detection of DNA and RNA. *Mol Biosyst* **2014,** *10* (5), 970-1003.

51. Xiao, Z.; Lie, P. C.; Fang, Z. Y.; Yu, L. X.; Chen, J. H.; Liu, J.; Ge, C. C.; Zhou, X. M.; Zeng, L. W., A lateral flow biosensor for detection of single nucleotide polymorphism by circular strand displacement reaction. *Chem Commun* **2012,** *48* (68), 8547-8549.

52. Liu, P.; Yang, X. H.; Sun, S.; Wang, Q.; Wang, K. M.; Huang, J.; Liu, J. B.; He, L. L., Enzyme-Free Colorimetric Detection of DNA by Using Gold Nanoparticles and Hybridization Chain Reaction Amplification. *Anal Chem* **2013,** *85* (16), 7689-7695.

53. Xu, W.; Xue, X. J.; Li, T. H.; Zeng, H. Q.; Liu, X. G., Ultrasensitive and Selective Colorimetric DNA Detection by Nicking Endonuclease Assisted Nanoparticle Amplification. *Angew Chem Int Edit* **2009,** *48* (37), 6849-6852.

54. Xu, Y.; Lunnen, K. D.; Kong, H. M., Engineering a nicking endonuclease N.AlwI by domain swapping. *P Natl Acad Sci USA* **2001,** *98* (23), 12990-12995.

55. Dirks, R. M.; Pierce, N. A., Triggered amplification by hybridization chain reaction. *P Natl Acad Sci USA* **2004,** *101* (43), 15275-15278.

56. Mou, F. Z.; Chen, C. R.; Zhong, Q.; Yin, Y. X.; Ma, H. R.; Guan, J. G., Autonomous Motion and Temperature-Controlled Drug Delivery of Mg/Pt-Poly(N-isopropylacrylamide) Janus Micromotors Driven by Simulated Body Fluid and Blood Plasma. *Acs Appl Mater Inter* **2014,** *6* (12), 9897-9903.

57. Thamphiwatana, S.; Fu, V.; Zhu, J. Y.; Lu, D. N.; Gao, W. W.; Zhang, L. F., Nanoparticle-Stabilized Liposomes for pH-Responsive Gastric Drug Delivery. *Langmuir* **2013,** *29* (39), 12228-12233.

58. Ma, H. C.; Fei, J. B.; Li, Q.; Li, J. B., Photo-induced Reversible Structural Transition of Cationic Diphenylalanine Peptide Self-Assembly. *Small* **2015,** *11* (15), 1787-1791.

59. Yan, Y.; Wang, H. B.; Li, B.; Hou, G. F.; Yin, Z. D.; Wu, L. X.; Yam, V. W. W., Smart Self-Assemblies Based on a Surfactant-Encapsulated Photoresponsive Polyoxometalate Complex. *Angew Chem Int Edit* **2010,** *49* (48), 9233-9236.

60. Boekhoven, J.; Brizard, A. M.; Kowlgi, K. N. K.; Koper, G. J. M.; Eelkema, R.; van Esch, J. H., Dissipative Self-Assembly of a Molecular Gelator by Using a Chemical Fuel. *Angew Chem Int Edit* **2010,** *49* (28), 4825-4828.

61. Grotsch, R. K.; Angi, A.; Mideksa, Y. G.; Wanzke, C.; Tena-Solsona, M.; Feige, M. J.; Rieger, B.; Boekhoven, J., Dissipative Self-Assembly of Photoluminescent Silicon Nanocrystals. *Angew Chem Int Edit* **2018,** *57* (44), 14608-14612.

62. Lin, Y. H.; Chang, C. H.; Wu, Y. S.; Hsu, Y. M.; Chiou, S. F.; Chen, Y. J., Development of pH-responsive chitosan/heparin nanoparticles for stomach-specific anti-Helicobacter pylori therapy. *Biomaterials* **2009,** *30* (19), 3332-3342.

63. Tocanne, J. F.; Teissie, J., Ionization of Phospholipids and Phospholipid-Supported Interfacial Lateral Diffusion of Protons in Membrane Model Systems. *Biochim Biophys Acta* **1990,** *1031* (1), 111-142.

64. Hafez, I. M.; Ansell, S.; Cullis, P. R., Tunable pH-sensitive liposomes composed of mixtures of cationic and anionic lipids. *Biophys J* **2000,** *79* (3), 1438-1446.

65. Furuta, T.; Graham, D. Y., Pharmacologic Aspects of Eradication Therapy for Helicobacter pylori Infection. *Gastroenterol Clin N* **2010,** *39* (3), 465-480.

66. Ragazzon, G.; Prins, L. J., Energy consumption in chemical fuel-driven self-assembly. *Nat Nanotechnol* **2018,** *13* (10), 882-889.

67. Tena-Solsona, M.; Wanzke, C.; Riess, B.; Bausch, A. R.; Boekhoven, J., Self-selection of dissipative assemblies driven by primitive chemical reaction networks. *Nat Commun* **2018,** *9*, 1-8.

68. Boekhoven, J.; Hendriksen, W. E.; Koper, G. J. M.; Eelkema, R.; van Esch, J. H., Transient assembly of active materials fueled by a chemical reaction. *Science* **2015,** *349* (6252), 1075-1079.

69. Leira-Iglesias, J.; Tassoni, A.; Adachi, T.; Stich, M.; Hermans, T. M., Oscillations, travelling fronts and patterns in a supramolecular system. *Nat Nanotechnol* **2018,** *13* (11), 1021-1027.

70. Kausar, A.; Mitran, C. J.; Li, Y. M.; Gibbs-Davis, J. M., Rapid, Isothermal DNA Self-Replication Induced by a Destabilizing Lesion. *Angew Chem Int Edit* **2013,** *52* (40), 10577-10581.

71. Alladin-Mustan, B. S.; Mitran, C. J.; Gibbs-Davis, J. M., Achieving room temperature DNA amplification by dialling in destabilization. *Chem Commun* **2015,** *51* (44), 9101-9104.

72. Esmaili, M.; Ghaffari, S. M.; Moosavi-Movahedi, Z.; Atri, M. S.; Sharifizadeh, A.; Farhadi, M.; Yousefi, R.; Chobert, J. M.; Haertle, T.; Moosavi-Movahedi, A. A., Beta casein-micelle as a nano vehicle for solubility enhancement of curcumin; food industry application. *Lwt-Food Sci Technol* **2011,** *44* (10), 2166-2172.

73. Gu, J. X.; Cheng, W. P.; Liu, J. G.; Lo, S. Y.; Smith, D.; Qu, X. Z.; Yang, Z. Z., pH-triggered reversible "stealth" polycationic micelles. *Biomacromolecules* **2008,** *9* (1), 255-262.

74. Guo, X. Z.; Song, J.; Ren, J.; Yang, F. E.; Kanamori, K.; Nakanishi, K., Facile preparation of well-defined macroporous yttria-stabilized zirconia monoliths via sol-gel process accompanied by phase separation. *J Porous Mat* **2016,** *23* (4), 867-875.

75. Merindol, R.; Walther, A., Materials learning from life: concepts for active, adaptive and autonomous molecular systems. *Chem Soc Rev* **2017,** *46* (18), 5588-5619.

76. Sorrenti, A.; Leira-Iglesias, J.; Markvoort, A. J.; de Greef, T. F. A.; Hermans, T. M., Non-equilibrium supramolecular polymerization. *Chem Soc Rev* **2017,** *46* (18), 5476-5490.

77. van Rossum, S. A. P.; Tena-Solsona, M.; van Esch, J. H.; Eelkema, R.; Boekhoven, J., Dissipative out-of-equilibrium assembly of man-made supramolecular materials. *Chem Soc Rev* **2017,** *46* (18), 5519-5535.

78. Riess, B.; Boekhoven, J., Applications of Dissipative Supramolecular Materials with a Tunable Lifetime. *Chemnanomat* **2018,** *4* (8), 710-719.

79. Debnath, S.; Roy, S.; Ulijn, R. V., Peptide Nanofibers with Dynamic Instability through Nonequilibrium Biocatalytic Assembly. *J Am Chem Soc* **2013,** *135* (45), 16789-16792.

80. Riess, B.; Wanzke, C.; Tena-Solsona, M.; Grotsch, R. K.; Maity, C.; Boekhoven, J., Dissipative assemblies that inhibit their deactivation. *Soft Matter* **2018,** *14* (23), 4852-4859.

81. Leira-Iglesias, J.; Sorrenti, A.; Sato, A.; Dunne, P. A.; Hermans, T. M., Supramolecular pathway selection of perylenediimides mediated by chemical fuels. *Chem Commun* **2016,** *52* (58), 9009-9012.

82. Sorrenti, A.; Leira-Iglesias, J.; Sato, A.; Hermans, T., Non-equilibrium steady states in supramolecular polymerization. *Abstr Pap Am Chem S* **2018,** *255*, 1-8

83. Maiti, S.; Fortunati, I.; Ferrante, C.; Scrimin, P.; Prins, L. J., Dissipative self-assembly of vesicular nanoreactors. *Nat Chem* **2016,** *8* (7), 725-731.

84. Tena-Solsona, M.; Riess, B.; Grotsch, R. K.; Lohrer, F. C.; Wanzke, C.; Kasdorf, B.; Bausch, A. R.; Muller-Buschbaum, P.; Lieleg, O.; Boekhoven, J., Non-equilibrium dissipative supramolecular materials with a tunable lifetime. *Nat Commun* **2017,** *8*, 1-8

85. Rostovtsev, V. V.; Green, L. G.; Fokin, V. V.; Sharpless, K. B., A stepwise Huisgen cycloaddition process: Copper(I)-catalyzed regioselective "ligation" of azides and terminal alkynes. *Angew Chem Int Edit* **2002,** *41* (14), 2596-2599.

86. Tornoe, C. W.; Christensen, C.; Meldal, M., Peptidotriazoles on solid phase: [1,2,3]-triazoles by regiospecific copper(I)-catalyzed 1,3-dipolar cycloadditions of terminal alkynes to azides. *J Org Chem* **2002,** *67* (9), 3057-3064.

87. Franc, G.; Kakkar, A., Dendrimer design using Cu(I)-catalyzed alkyne-azide "click-chemistry". *Chem Commun* **2008,** (42), 5267-5276.

88. Mullen, D. G.; McNerny, D. Q.; Desai, A.; Cheng, X. M.; DiMaggio, S. C.; Kotlyar, A.; Zhong, Y.; Qin, S.; Kelly, C. V.; Thomas, T. P.; Majoros, I.; Orr, B. G.; Baker, J. R.; Holl, M. M. B., Design, Synthesis, and Biological Functionality of a Dendrimer-Based Modular Drug Delivery Platform. *Bioconjugate Chem* **2011,** *22* (4), 679-689.

89. Gilles, M. A.; Hudson, A. Q.; Borders, C. L., Stability of Water-Soluble Carbodiimides in Aqueous-Solution. *Anal Biochem* **1990,** *184* (2), 244-248.

90. Zemlyanov, A. A.; Geints, Y. E.; Pal'chikov, A. V., Dynamic light scattering on stimulated droplet surface vibrations caused by high power laser radiation: particle sizing. *P Soc Photo-Opt Ins* **2000,** *4341*, 185-193.

91. Soderman, O.; Stilbs, P.; Price, W. S., NMR studies of surfactants. *Concept Magn Reson A* **2004,** *23a* (2), 121-135.

92. Oishi, M.; Sugiyama, S., An Efficient Particle-Based DNA Circuit System: Catalytic Disassembly of DNA/PEG-Modified Gold Nanoparticle-Magnetic Bead Composites for Colorimetric Detection of miRNA. *Small* **2016,** *12* (37), 5153-5158.

93. Wang, G. Q.; Akiyama, Y.; Shiraishi, S.; Kanayama, N.; Takarada, T.; Maeda, M., Cross-Linking versus Non-Cross-Linking Aggregation of Gold Nanoparticles Induced by DNA Hybridization: A Comparison of the Rapidity of Solution Color Change. *Bioconjugate Chem* **2017,** *28* (1), 270-277.

94. Nam, J. M.; Thaxton, C. S.; Mirkin, C. A., Nanoparticle-based bio-bar codes for the ultrasensitive detection of proteins. *Science* **2003,** *301* (5641), 1884-1886.

95. Zhang, H. Q.; Lai, M. D.; Zuehlke, A.; Peng, H. Y.; Li, X. F.; Le, X. C., Binding-Induced DNA Nanomachines Triggered by Proteins and Nucleic Acids. *Angew Chem Int Edit* **2015,** *54* (48), 14326-14330.

96. Lee, J. S.; Han, M. S.; Mirkin, C. A., Colorimetric detection of mercuric ion (Hg^{2+}) in aqueous media using DNA-functionalized gold nanoparticles. *Angew Chem Int Edit* **2007,** *46* (22), 4093-4096.

97. Ye, B. C.; Yin, B. C., Highly Sensitive Detection of Mercury(II) Ions by Fluorescence Polarization Enhanced by Gold Nanoparticles. *Angew Chem Int Edit* **2008,** *47* (44), 8386-8389.

98. Leng, B.; Zou, L.; Jiang, J. B.; Tian, H., Colorimetric detection of mercuric ion (Hg2+) in aqueous media using chemodosimeter-functionalized gold nanoparticles. *Sensor Actuat B-Chem* **2009,** *140* (1), 162-169.

99. Rosi, N. L.; Mirkin, C. A., Nanostructures in biodiagnostics. *Chem Rev* **2005,** *105* (4), 1547-1562.

100. Quinn, J. F.; Patel, T.; Wong, D.; Das, S.; Freedman, J. E.; Laurent, L. C.; Carter, B. S.; Hochberg, F.; Van Keuren-Jensen, K.; Huentelman, M.; Spetzler, R.; Kalani, M. Y. S.; Arango, J.; Adelson, P. D.; Weiner, H. L.; Gandhi, R.; Goilav, B.; Putterman, C.; Saugstad, J. A., Extracellular RNAs: development as biomarkers of human disease. *J Extracell Vesicles* **2015,** *4*, 1-16.

101. Islam, M. N.; Masud, M. K.; Haque, M. H.; Al Hossain, M. S.; Yamauchi, Y.; Nguyen, N. T.; Shiddiky, M. J. A., RNA Biomarkers: Diagnostic and Prognostic Potentials and Recent Developments of Electrochemical Biosensors. *Small Methods* **2017,** *1* (7), 1700131.

102. Fleming, A. M.; Ding, Y.; Alenko, A.; Burrows, C. J., Zika Virus Genomic RNA Possesses Conserved G-Quadruplexes Characteristic of the Flaviviridae Family. *Acs Infect Dis* **2016,** *2* (10), 674-681.

103. Lam, M. K.; Gadzikwa, T.; Nguyen, T.; Kausar, A.; Alladin-Mustan, B. S.; Sikder, M. D.; Gibbs-Davis, J. M., Tuning Toehold Length and Temperature to Achieve Rapid, Colorimetric

Detection of DNA from the Disassembly of DNA-Gold Nanoparticle Aggregates. *Langmuir* **2016,** *32* (6), 1585-1590.

104. Dong, H. F.; Lei, J. P.; Ding, L.; Wen, Y. Q.; Ju, H. X.; Zhang, X. J., MicroRNA: Function, Detection, and Bioanalysis. *Chem Rev* **2013,** *113* (8), 6207-6233.

105. Kausar, A.; McKay, R. D.; Lam, J.; Bhogal, R. S.; Tang, A. Y.; Gibbs-Davis, J. M., Tuning DNA Stability To Achieve Turnover in Template for an Enzymatic Ligation Reaction. *Angew Chem Int Edit* **2011,** *50* (38), 8922-8926.

106. Kibbe, W. A., OligoCalc: an online oligonucleotide properties calculator. *Nucleic Acids Res* **2007,** *35*, W43-W46.

107. Enustun, B. V.; Turkevich, J., Coagulation of Colloidal Gold. *J Am Chem Soc* **1963,** *85* (21), 3317-3328.

108. Kimling, J.; Maier, M.; Okenve, B.; Kotaidis, V.; Ballot, H.; Plech, A., Turkevich method for gold nanoparticle synthesis revisited. *J Phys Chem B* **2006,** *110* (32), 15700-15707.

109. Sikder, M. D. H.; Gibbs-Davis, J. M., The Influence of Gap Length on Cooperativity and Rate of Association in DNA-Modified Gold Nanoparticle Aggregates. *J Phys Chem C* **2012,** *116* (21), 11694-11701.

110. Hurst, S. J.; Lytton-Jean, A. K. R.; Mirkin, C. A., Maximizing DNA loading on a range of gold nanoparticle sizes. *Anal Chem* **2006,** *78* (24), 8313-8318.

111. Stoeva, S. I.; Lee, J. S.; Thaxton, C. S.; Mirkin, C. A., Multiplexed DNA detection with biobarcoded nanoparticle probes. *Angew Chem Int Edit* **2006,** *45* (20), 3303-3306.

112. Kausar, A.; Osman, E. A.; Gadzikwa, T.; Gibbs-Davis, J. M., The presence of a 5 '-abasic lesion enhances discrimination of single nucleotide polymorphisms while inducing an isothermal ligase chain reaction (vol 141, pg 4272, 2016). *Analyst* **2017,** *142* (15), 2848-2848.

113. Mabey, D.; Peeling, R. W.; Ustianowski, A.; Perkins, M. D., Diagnostics for the developing world. *Nat Rev Microbiol* **2004,** *2* (3), 231-240.

114. LaBarre, P.; Boyle, D.; Hawkins, K.; Weigl, B., Instrument-free nucleic acid amplification assays for global health settings. *Proc Spie* **2011,** *8029*, 1-15.

115. Ribeiro, J. M. C.; Endris, T. M.; Endris, R., Saliva of the Soft Tick, Ornithodoros-Moubata, Contains Antiplatetlet and Apyrase Activities. *Comp Biochem Phys A* **1991,** *100* (1), 109-112.